Petrology, Vol. 11, No. 3, 2003, pp. 261–290. Translated from Petrologiya, Vol. 11, No. 3, 2003, pp. 289–320.

The Hisovaara Structure in the Northern Karelian Greenstone Belt as a Late Archean Accreted Island Arc: Isotopic Geochronological and Petrological Evidence

E. V. Bibikova*, A. V. Samsonov, A. A. Shchipansky***, M. M. Bogina**, T. V. Gracheva*, and V. A. Makarov***

** Vernadsky Institute of Geochemistry and Analytical Chemistry, Russian Academy of Sciences, ul. Kosygina 19, Moscow, 117975 Russia; e-mail: elkor@geokhi.msk.ru*
*** Institute of the Geology of Ore Deposits, Petrography, Mineralogy, and Geochemistry, Russian Academy of Sciences, Staromonetnyi per. 35, Moscow, 109017 Russia; e-mail: samsonov@igem.ru*
**** Geological Institute, Russian Academy of Sciences, Pyzhevskii per. 7, Moscow, 109017 Russia*
Received November 6, 2002

Abstract—The Hisovaara structure in the northern Karelian greenstone belt includes two complexes of metamorphosed magmatic rocks different in age and composition. The earlier of them comprises metamorphosed tholeiites, boninites, ferrobasalts (Shchipansky *et al.*, 2002), and andesites of the tholeiite series. According to the assemblage of rocks and their petrochemical characteristics, this complex is analogous to associations of Phanerozoic initial oceanic island arcs. The other, younger, complex consists of three petrogenetic rock groups of volcanic, subvolcanic, and plutonic facies, including (1) tonalites, trondhjemites, dacites, and rhyolites of the adakite series; (2) andesite–dacites of the calc–alkaline series; and (3) Nb–Ti andesites. The U–Pb dating of magmatic zircon from the rocks of this complex from different parts of the structure gives similar (within the instrumental error) age values in the range of 2.82–2.78 Ga. This fact highlights the closely coeval origin of volcano-plutonic series in the Hisovaara structure within the framework of a single tectono-magmatic event. The subduction-related nature of the latter is determined by the analogy between these rock complexes and magmatic association in some modern island arcs, where the subduction of young hot plates brings about a thermal regime that was also suggested for Archean subduction zones. The comparative analysis of the petro- and geochemical characteristics and geochronologic data reveals significant differences between the ages of compositionally similar metavolcanics with island-arc signatures in two structures of the northern Karelian belt: Hisovaara (2.78–2.82 Ga) and Keret' (2.82–2.88 Ga; Bibikova *et al.*, 1999a). This makes it possible to regard the northern Karelian belt as an accretionary structure in which associations of at least two island arcs of different ages are combined.

INTRODUCTION

The Karelian gneiss (granite)–greenstone terrane (GGT) consists of extensive granite-gneiss areas and volcano-sedimentary sequences of greenstone belts (Fig. 1, references in the capture to it). The geologic history of the Karelia GGT is subdivided into three stages. The earlier of them ("pregreenstone" stage at 3.1–3.2 Ga) was responsible for the origin of the early sialic crust, whose fragments are preserved as spatially separated and extensively recycled blocks in eastern Karelia, eastern Finland, and, possibly, also in western Karelia. During the later ("greenstone" proper) stage at 2.94–2.78 Ga, supracrustal sequences of greenstone belts were formed, along with the related granitoids of the tonalite–trondhjemite–granodiorite (TTG) series. The third stage ("cratonization" at 2.74–2.69 Ga) was marked by the massive intrusion of late- and postkinematic magnesian monzodiorites (sanukitoids), subalkaline and alkaline granites, and lamprophyre dikes, which were the last in the Archean evolution of the Karelian GGT. As a result, a consolidated crustal block was produced late in the Archean, and it responded as a brittle body to Paleoproterozoic rifting starting from 2.5 Ga (Shcheglov *et al.*, 1993; Lobach-Zhuchenko *et al.*, 1998).

The key problems in reconstructing the Archean evolution of the Karelian GGT are the tectonic environments in which the supracrustal rocks and granitoids of the TTG–greenstone complex were produced. The metamorphosed rocks are restricted to relatively small structures, whose adjacent chains are combined into a number of greenstone belts (Sokolov, 1981). All of the belts include two principal associations of supracrustal rocks: (1) metavolcanics of mafic and ultramafic composition and associated chemogenic sediments and (2) metamorphosed volcanics and tuff-sedimentary rocks of andesite–dacite–rhyolite composition in association with chemogenic and terrigenous sediments. The rocks framing the structures ubiquitously include TTG-granitoids, which are in either intrusive or tectonic contacts with the neighboring supracrustal rocks.

SAMPLE PREPARATION AND THE METHODS OF THE PETROCHEMICAL AND ISOTOPIC GEOCHRONOLOGIC STUDIES

The samples (300–500 g) selected for the petrogeochemical examination were crushed, quartered, and pulverized at the Laboratory of Mineralogical Analysis of the Institute of the Lithosphere, Russian Academy of Sciences. Major elements were determined by XRF on a VRA-20R spectrometer at the Institute of Geology, Geophysics, and Mineralogy, Siberian Division, Russian Academy of Sciences, in Novosibirsk. Trace elements were determined by ICP-MS at the Institute of Mineralogy, Geochemistry, and Crystal Chemistry of Rare Elements (analyst D.Z. Zhuravlev). The geochemical simulation of equilibrium partial melting and fractional crystallization was conducted by formulas from (Rollinson, 1993) with the use of average mineral/melt partition coefficients borrowed from the same paper (pp. 108–111).

Accessory zircon was derived from 10- to 15-kg samples following the conventional procedure, involving a combination of magnetic separation and the use of bromoform, at the Laboratory of Mineralogical Analysis of the Institute of the Lithosphere, Russian Academy of Sciences. Monomineralic zircon samples for isotopic analysis were prepared by hand-picking under a binocular magnifier. The morphology and inner structure of zircon crystals were inspected in transmitted and reflected light under a polarization microscope in air and alcohol. The U–Pb isotopic study of the zircon was conducted at the Isotopic Laboratory of Vernadsky Institute of Geochemistry and Analytical Chemistry, Russian Academy of Sciences, by the procedure adopted at this laboratory. Zircon samples 0.5–3 mg in weight were decomposed, and U and Pb were extracted from them for the isotopic study by the technique described in (Krogh, 1973). The U and Pb concentrations were determined by isotopic dilution with the use of a mixed $^{208}Pb + {}^{235}U$ tracer. The total blank did not exceed 0.1–0.2 ng Pb. The Pb isotopic composition was measured on a CAMECA TSN 206A one-collector solid-state mass spectrometer. Age corrections for common Pb were introduced in compliance with the model of Stacey and Kramers (1975). The isotopic data regression was calculated by the computer program of Ludwig (1991) with the modern decay constants from (Steiger and Jaeger, 1976). The inaccuracy of the U–Pb isotopic ratios was 0.5%. To enhance the concordancy of the isotopic ages, the most disturbed zircon phases from some fractions were selectively leached (SL) by an acid (Mattison, 1994). The zircon was preliminarily treated by concentrated HF in a thermostat at a temperature of 150°C for 8 h, after which the cooled solution was decanted and the crystalline residue was doubly treated by 3.1 N HCl solution at temperatures of 180 and 200°C for 10 h. The HCl solution was decanted, the residue was doubly washed with concentrated HNO_3, after which the crystalline zircon residue was decomposed following the conventional procedure. Some zircon fractions were preliminarily air-abraded by the method described in (Krogh, 1982). For one sample (7/96), from which we managed to obtain only a few zircon crystals, the U–Th–Pb isotopic study was conducted at the Isotopic Laboratory of the Swedish Museum of Natural History, Stockholm, on a CAMECA 1270 ion microprobe at the Nordsim Laboratory under the supervision of Dr. M. Whitehouse. Zircon grains to be analyzed were mounted, along with a reference zircon, in epoxy pellets, which were then polished until the crystal cores were exposed. The inner structure of the zircon grains was preliminarily examined by CL. Before the analysis, the pellet was sputter coated with Au. The primary ion beam of O_2^- ions first affected an ellipsoidal 25×40 μm area of the crystal. The secondary ions were analyzed at a mass resolving power of 5600, which enabled the resolution of all the atomic masses of interest. The reader can find more details of the analytical procedure in (Whitehouse *et al.*, 1997). The Pb isotopic analyses were accurate to 0.1–0.3%, and the U–Pb isotopic ratios were measured accurate to 1–3%.

GEOCHEMISTRY OF THE INTERMEDIATE AND ACID VOLCANIC ROCKS OF THE HISOVAARA STRUCTURE AND THE TTG GRANITOIDS FRAMING IT

The aforementioned tectonic and compositional asymmetry of the Hisovaara structure is also accentuated by the petro- and geochemical differences between the intermediate and acid metavolcanics and TTG granitoids in its northern and southern parts.

Northern Part of the Structure

Metavolcanics of intermediate composition, transformed into biotite–quartz–amphibole–plagioclase schists, correspond to low-Al high-Fe Na-basaltic andesite and andesite (SiO_2 = 53–64 wt %), which plot within the fields of both calc-alkaline and tholeiitic series in classification diagrams (Fig. 5). According to their petrochemistry, the andesites can be subdivided into three groups (Table 1, Figs. 6–8). Andesites 1 are volumetrically dominant and have lower concentrations of HFSE and REE and weakly fractionated LREE and HREE patterns with negative Eu anomalies [$(La/Sm)_N$ = 0.79–1.9, $(Gd/Yb)_N$ = 1.5–1.9, Eu/Eu* = 0.82–0.94] and small negative anomalies at Nb and Ti. Andesites 2 are localized within stripes of variable thickness in the northern and southern flanks of the andesite unit. They are close to "primitive" andesites in terms of major-element concentrations but are strongly enriched in LREE [$(La/Sm)_N$ = 3.3–4.1, $(Gd/Yb)_N$ = 1.7–2.1, Eu/Eu* = 0.81–0.92] at somewhat higher concentrations of HREE and HFSE and significant negative anomalies at Nb and Ti. Andesites 3 compose a thin bed in the southern part of the andesite unit and are characterized by high concentrations of Fe_2O_3, TiO_2,

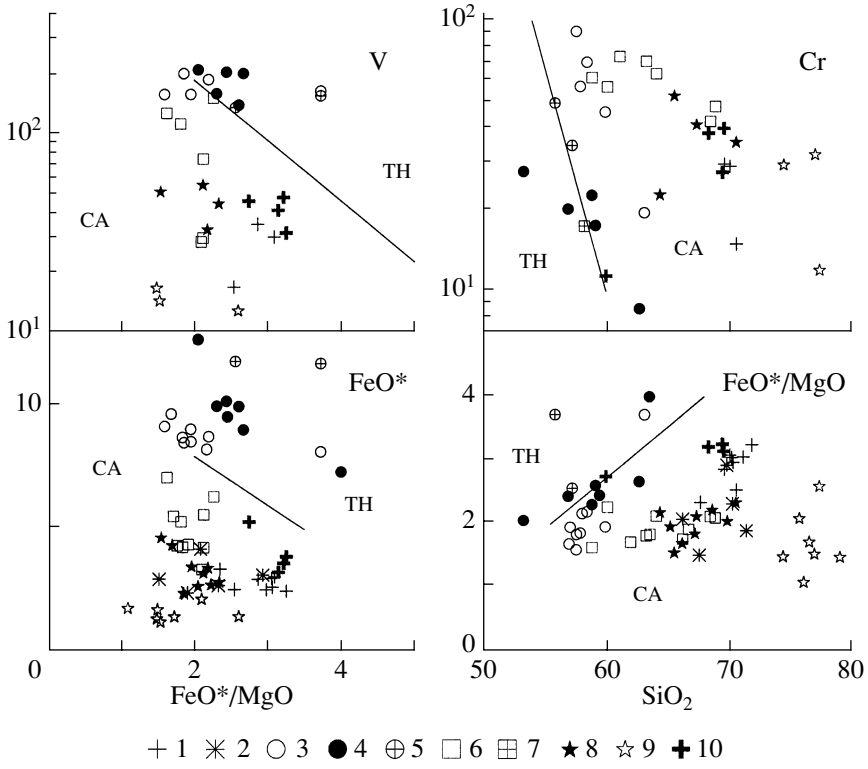

Fig. 5. Classification petrochemical diagrams for the intermediate and acid magmatic rocks of the Hisovaara structure.
Northern portion of the structure: (1) peripheral trondhjemite, (2) subvolcanic rhyodacite. Tholeiitic: (3) andesite 1, (4) andesite 2, (5) andesite 3. **Southern portion of the structure:** (6) calc–alkaline andesite and dacite, (7) Nb–Ti andesite, (8) subvolcanic rhyodacite, (9) subvolcanic rhyolite, (10) rhyolite and granodiorite. The boundary lines between the calc–alkaline (CA) and tholeiitic (TH) series are after (Miyashiro, 1974, 1975).

Zr, and Nb at low concentrations of MgO, elevated concentrations of REE with moderately fractionated LREE and HREE patterns [$(La/Sm)_N$ = 2.8–3.0, $(Gd/Yb)_N$ = 2.3–2.5, Eu/Eu* = 0.84–0.91], and unclear negative anomalies at Nb.

Granitoids framing the structure in the north and subvolcanic rhyodacites, which occur among the mafic rocks, show similar petrochemical characteristics and correspond to calc–alkaline high-Al trondhjemite with high Sr and low Y and HREE concentrations, and strongly fractionated REE patterns [$(La/Sm)_N$ = 4.6–5.3, $(Gd/Yb)_N$ = 3.6–3.8] with relatively small Eu anomalies [Eu/Eu* = 0.94–1.03] and clearly pronounced negative Nb anomalies (Table 1, Figs. 5–8).

Southern Part of the Structure

Metavolcanics of intermediate and acid composition, transformed into fine-grained amphibole–biotite–quartz–plagioclase schists, correspond to high-Al calc–alkaline Na- and Na–K-andesites and dacites (Table 1, Figs. 5–7, 9), and most of their petrochemical characteristics principally differ from those of tholeiitic andesites in the northern portion of the structure. Most of these rocks lie on the same composition variation trends, with an increase in SiO_2 from 59 to 69 wt % associated with a decrease in the concentrations of TiO_2, Al_2O_3, Fe_2O_3, MgO, CaO, Cr, Ni, S, and Sr and an increase in the contents of Nb and Zr at decreasing concentrations of both LREE and HREE at their stronger fractionation and unsystematic variations in the Eu anomalies [Eu/Eu* = 0.88–1.15]. The metavolcanics of one area include schists whose composition corresponds to Nb–Ti andesite with elevated concentrations of Fe_2O_3, TiO_2 (1.34 wt %), Nb (11 ppm), and Zr at moderately fractionated REE patterns [$(La/Sm)_N$ = 2.5, $(Gd/Yb)_N$ = 1.9] and small negative Nb anomalies.

The **subvolcanic rocks** among mafic and intermediate–acid metavolcanics in the southern part of the structure correspond to calc–alkaline rhyodacites and rhyolites. The rhyodacites (SiO_2 = 64–70 wt %) are sodic high-Al rocks, enriched in Sr and depleted in Nb, Y, and HREE with strongly fractionated patterns of LREE and HREE [$(La/Sm)_N$ = 3.8–4.3, $(Gd/Yb)_N$ = 3.1–3.5, Eu/Eu* = 0.96–1.3] and pronounced negative anomalies at Nb (Table 1, Figs. 6, 8). All characteristics of these rhyodacites are very close to those of trondhjemites and subvolcanic rhyodacites in the northern part of the structure. The acid (SiO_2 = 74–79) K–Na rhyolites are characterized by elevated concentrations of U, Th, and Nb, are strongly enriched in LREE, and depleted in HREE [$(La/Sm)_N$ = 5.5–6.5, $(Gd/Yb)_N$ = 3.3–

Table 1. Average representative analyses of main rock types in the Hisovaara structure

Component	*1*	*2*	*3*	*4*	*5*	*6*	***7***	*8*	*9*	*10*
			N-321	N-334/1		Kh-14/96	**Kh-15/96**	Kh-19/96	Kh-23/96	Kh-3/96
SiO_2	50.76	51.93	56.77	60.14	49.55	69.67	**70.64**	70.12	71.48	58.87
TiO_2	0.84	1.07	0.42	0.36	1.98	0.38	**0.33**	0.37	0.31	0.79
Al_2O_3	15.13	14.54	11.73	10.05	14.03	15.70	**15.93**	15.67	15.73	14.16
Fe_2O_3	12.15	13.69	10.86	10.02	16.93	3.27	**2.81**	3.38	2.65	11.14
MnO	0.18	0.20	0.17	0.16	0.20	0.12	**0.11**	0.13	0.12	0.17
MgO	8.62	7.46	9.13	9.16	5.75	1.03	**0.99**	0.98	1.26	4.34
CaO	10.83	9.47	10.15	9.31	9.08	3.63	**3.34**	3.25	2.96	4.79
Na_2O	1.12	1.23	0.55	0.66	2.10	4.48	**4.11**	4.31	3.26	4.37
K_2O	0.29	0.27	0.16	0.07	0.18	1.54	**1.58**	1.65	2.09	1.16
P_2O_5	0.08	0.13	0.05	0.07	0.19	0.17	**0.15**	0.14	0.14	0.20
Li	20.2	18.8	23.30	30.4	19	42.4	**42.1**	42.2		35.8
Sc	41.90	41.3	36.3	46.4	28.2	5.26	**4.26**	5.10		27.8
Ti	5023	5812	2500	2186	11882	2003	**1888**	1940		4530
V	206	299	104	223	285	35.5	**17.2**	30.7		162
Cr	269	290	762	919	154	29.5	**15.0**	28.9		22.6
Co	48.4	50	306	191	48.3	7.98	**6.65**	6.91		39.5
Ni	112	112	77.6	62.3	46.0	16.4	**12.0**	16.4		47.1
Cu	73.58	27	49.8	27.3	86.7	8.7	**5.7**	14.9		60.7
Zn	80.0	99	86.7	65.3	105	52.5	**41.5**	58.6		87.8
Ga	14.5	18	11.5	9.56	19.3	21.5	**18.0**	21.2		18.5
Rb	10.1	7.48	2.25	0.74	2.05	44.1	**20.5**	38.7		33.5
Sr	99	97	82.5	73.5	248	477	**451**	468		208
Y	23.0	23.5	11	14.5	30.4	6	**4**	6		20
Zr	14.2	52.2	20.0	26.5	111	105	**118**	110	106	130
Nb	2.29	2.81	0.754	0.865	10.3	4	**4**	4		6
Cs	0.48	0.14	0.123	0.053	0.083	3	**2**	2		3
Ba	42	106	59.2	31.5	47	435	**427**	402		447
La	3.45	2.67	1.04	1.34	13.3	20.8	**15.9**	20.6	12.5	28.5
Ce	9.12	7.45	2.84	3.59	32.7	37.2	**28.5**	39.0	25.3	56.8
Pr	1.40	1.27	0.425	0.54	4.69	4.47	**4.11**	4.64	2.76	6.85
Nd	7.03	6.90	2.38	2.95	21.2	15.6	**14.5**	16.3	9.6	26.2
Sm	2.41	2.30	0.9	1.06	5.35	2.47	**2.19**	2.70	1.63	4.62
Eu	0.75	0.72	0.402	0.372	1.59	0.705	**0.594**	0.723	0.320	1.30
Gd	2.98	3.09	1.27	1.54	5.94	1.78	**1.66**	2.04	1.01	4.32
Tb	0.52	0.53	0.27	0.28	0.93	0.227	**0.173**	0.259	0.130	0.611
Dy	3.70	3.77	1.83	2.2	5.77	1.13	**0.74**	1.18	0.59	3.14
Ho	0.81	0.86	0.433	0.5	1.19	0.185	**0.162**	0.207	0.120	0.640
Er	2.38	2.46	1.2	1.42	3.2	0.422	**0.462**	0.506	0.220	1.780
Tm	0.34	0.37	0.194	0.216	0.44	0.059	**0.048**	0.073	0.030	0.237
Yb	2.22	2.32	1.22	1.48	2.65	0.383	**0.375**	0.449	0.260	1.63
Lu	0.33	0.35	0.174	0.259	0.38	0.061	**0.042**	0.065	0.040	0.223
Hf	0.61	1.63	0.62	0.75	2.90	2.87	**2.68**	2.53		3.56
Ta	0.13	0.61	0.188	0.056	0.63	0.219	**0.212**	0.298		0.374
Pb	1.72	1.75	3.07	0.896	2.22	6.33	**4.19**	6.78		9.91
Th	0.29	0.27	0.082	0.065	1.09	2.70	**1.99**	2.89		5.97
U	0.06	0.07	0.038	0.008	0.23	0.582	**0.508**	0.609		0.928
$(La/Yb)_N$	1.07	0.79	0.58	0.61	3.05	36.8	**28.6**	31.0	32.5	11.8
$(La/Sm)_N$	0.92	0.74	0.73	0.80	1.40	5.30	**4.57**	4.81	4.83	3.88
$(Gd/Yb)_N$	1.09	1.10	0.84	0.84	1.72	3.76	**3.58**	3.67	3.14	2.14
Eu/Eu*	0.86	0.83	1.15	0.89	0.88	1.03	**0.95**	0.94	0.76	0.89

Table 1. (Contd.)

Component	*11*	*12*	*13*	*14*	*15*	*16*	*17*	*18*	*19*	*20*
	Kh-7/96	Kh-27-2/96	Kh-42/96	K-77/97	Kh-8/96	Kh-28/96	Kh-35/96	Kh-36/96	Kh-38/96	Kh-39/96
SiO_2	**53.31**	62.70	56.94	59.16	57.11	57.60	59.95	58.47	57.92	63.13
TiO_2	**0.85**	0.86	0.83	0.81	0.67	0.63	0.73	0.71	0.66	0.67
Al_2O_3	**15.60**	13.51	14.60	14.26	14.42	14.40	14.00	13.98	15.08	12.75
Fe_2O_3	**14.17**	10.08	11.36	11.13	10.12	10.24	9.54	9.78	9.50	9.09
MnO	**0.16**	0.15	0.17	0.17	0.17	0.17	0.16	0.18	0.17	0.16
MgO	**6.19**	3.40	4.19	3.84	5.21	5.18	3.96	4.79	4.37	3.72
CaO	**4.95**	4.60	5.08	5.36	5.85	5.78	6.44	6.40	6.47	5.44
Na_2O	**4.44**	4.45	4.93	4.40	6.06	5.70	4.74	5.27	5.38	4.56
K_2O	**0.13**	0.09	1.68	0.72	0.22	0.09	0.27	0.17	0.19	0.29
P_2O_5	**0.19**	0.15	0.20	0.16	0.18	0.21	0.20	0.25	0.25	0.20
Li	**20.1**	8.21	23.1	21.4		9.72	6.44	4.65	4.83	4.88
Sc	**22.7**	22.5	19.8	24.5		26.4	23.5	24.3	21.4	18.8
Ti	**4770**	4800	4660	4152		3505	4043	3740	3970	3520
V	**214**	205	208	142		161	161	191	205	167
Cr	**27.6**	8.62	20.1	17.5		91.5	46.0	70.4	57.2	19.5
Co	**40.9**	28.6	32.9	33.3		40.7	31.0	35.8	21.6	30.0
Ni	**47.6**	23.4	40.7	36.5		52.3	35.5	52.1	41.9	40.6
Cu	**69.2**	87.2	36.3	53.6		12.2	7.72	4.66	9.52	16.7
Zn	**131**	127	83.3	81.2		69.6	63.4	83.1	73.5	55.7
Ga	**21.7**	19	16.7	17.5		18.8	19.3	19.2	17.5	16.9
Rb	**2.11**	0	40.1	22.1		1.39	2.89	0.50	0.53	0.98
Sr	**76**	76	137	216		164	405	138	238	112
Y	**16**	18	15	20		17.9	19.2	11.7	14.0	12.2
Zr	**133**	134	129	124	109	105	121	105	100	113
Nb	**6**	6	5	6		4.24	6.74	4.67	5.16	4.47
Cs	**0**	0	1	1		0	0	0	0	0
Ba	**54**	45	547	239		42.8	43.9	26.0	35.9	49.6
La	**23.3**	24.6	22.6	28.3	6.69	3.75	6.35	5.98	7.86	8.91
Ce	**48.1**	53.3	46.8	55.6	16.5	11.0	16.1	19.5	21.10	22.9
Pr	**5.61**	6.33	5.55	6.59	2.31	2.04	2.77	2.64	3.16	3.21
Nd	**21.8**	23.8	22.4	23.7	10.0	10.8	12.5	11.4	14.40	13.50
Sm	**4.14**	4.71	4.06	4.38	2.56	2.98	3.00	2.67	3.38	3.00
Eu	**1.09**	1.30	1.13	1.09	0.750	0.804	0.868	0.711	0.991	0.781
Gd	**3.45**	4.00	3.58	3.89	2.46	3.02	3.08	2.33	3.08	2.61
Tb	**0.589**	0.629	0.541	0.560	0.370	0.410	0.460	0.399	0.461	0.422
Dy	**2.78**	3.54	2.73	3.16	2.09	2.72	3.00	2.26	2.66	2.23
Ho	**0.597**	0.723	0.556	0.614	0.430	0.543	0.634	0.439	0.565	0.486
Er	**1.66**	1.95	1.48	1.96	1.20		1.71	1.27	1.49	1.25
Tm	**0.252**	0.316	0.259	0.273	0.180	0.214	0.260	0.205	0.203	0.200
Yb	**1.62**	1.84	1.46	1.65	1.17	1.37	1.50	1.27	1.34	1.18
Lu	**0.196**	0.259	0.181	0.249	0.170	0.192	0.214	0.160	0.193	0.171
Hf	**2.85**	3.34	2.94	3.56		2.84	3.50	2.12	1.89	2.83
Ta	**0.368**	0.408	0.370	0.370		0.196	0.317	0.336	0.298	0.297
Pb	**5.08**	7.04	8.71	9.36		4.97	4.58	2.95	5.40	8.76
Th	**6.08**	6.02	5.02	5.77		3.76	5.80	3.32	4.00	4.62
U	**0.821**	0.989	0.931	0.959		0.622	1.08	0.77	0.797	0.981
$(La/Yb)_N$	**9.71**	9.02	10.4	11.6	3.86	1.85	2.86	3.18	3.96	5.10
$(La/Sm)_N$	**3.54**	3.29	3.50	4.07	1.65	0.79	1.33	1.41	1.46	1.87
$(Gd/Yb)_N$	**1.72**	1.76	1.98	1.91	1.70	1.78	1.67	1.48	1.86	1.79
Eu/Eu*	**0.88**	0.92	0.91	0.81	0.91	0.82	0.87	0.87	0.94	0.85

Table 1. (Contd.)

Component	*21*	*22*	*23*	*24*	*25*	*26*	*27*	***28***	*29*	*30*
	Kh-1/96	K-78/97	K-37B/97	K-29/97	K-30A/97	K-30D/97	K-36/97	**K-76/97**	K-74/97	K-38/97
SiO_2	55.87	57.27	58.27	58.90	63.31	60.16	64.13	**68.53**	68.94	64.42
TiO_2	1.57	1.62	1.34	0.70	0.75	0.85	0.59	**0.57**	0.45	0.41
Al_2O_3	14.97	14.05	17.42	16.35	17.02	17.52	17.25	**15.51**	16.19	16.79
Fe_2O_3	13.08	13.17	8.87	7.92	5.91	7.04	6.23	**4.72**	3.72	3.79
MnO	0.17	0.18	0.16	0.17	0.16	0.22	0.15	**0.13**	0.12	0.18
MgO	3.16	3.18	3.77	4.37	2.93	2.79	2.63	**2.00**	1.59	1.56
CaO	6.26	5.39	4.59	7.68	4.74	6.16	3.64	**3.52**	3.75	7.91
Na_2O	4.36	4.69	2.49	2.42	2.79	2.76	3.38	**3.81**	3.34	3.41
K_2O	0.26	0.21	2.89	1.28	2.19	2.28	1.90	**1.10**	1.76	1.40
P_2O_5	0.29	0.23	0.20	0.20	0.18	0.22	0.10	**0.11**	0.14	0.13
Li	25.0	14.8	32.7	15.2	13.4	13.8	15.1	**10.3**	12.6	13.5
Sc	17.3	17.1	15.6	15.9	12.5	17.3	10.7	**7.43**	7.08	6.97
Ti	9650	9147	7197	3780	3660	4520	2520	**2928**	2246	1690
V	158	138	72.6	129	114	154	75.6	**30.3**	29.0	33.3
Cr	49.7	34.5	17.4	61.7	71.0	57.0	63.9	**42.5**	48.3	22.7
Co	47.6	47.3	15.6	21.3	14.6	12.7	8.20	**12.1**	10.4	10.9
Ni	81.0	65.9	20.3	38.3	35.4	24.0	21.7	**36.7**	37.2	24.2
Cu	219	158	8.20	8.79	10.7	6.17	9.07	**10.20**	13.4	9.37
Zn	106	152	144	96.8	78.3	87.1	60.7	**68.3**	43.3	77.8
Ga	21.0	20.3	18.8	21.1	20.6	19.9	19.1	**18.2**	17.4	18.0
Rb	3.23	2.95	98.6	28.8	61.7	59.8	51.7	**26.5**	47.0	36.9
Sr	239	329	313	567	457	366	235	**231**	205	618
Y	21.9	24.6	18.9	12.9	10.4	11.9	8.63	**9.96**	5.79	6.20
Zr	162	155	145	96	125	115	139	**140**	134	83.0
Nb	13.40	13.3	11.3	2.69	4.80	3.71	4.50	**7.02**	4.46	1.99
Cs	0	0	3.35	1.52	2.47	2.11	3.73	**0.70**	1.31	3.42
Ba	82.8	175	639	428	815	642	487	**272**	512	297
La	31.5	32.8	16.8	17.3	22.8	21.7	10.7	**14.5**	13.4	14.3
Ce	65.7	70.3	37.6	38.3	48.2	47.4	23.4	**23.3**	20.4	26.6
Pr	8.63	9.23	4.79	4.81	5.94	6.04	2.72	**3.69**	3.00	3.17
Nd	34.70	36.10	19.20	21.10	24.00	24.60	10.00	**13.40**	10.00	11.30
Sm	6.53	7.28	4.28	4.16	4.46	4.69	1.87	**3.05**	1.79	2.07
Eu	1.81	1.85	1.13	1.16	1.25	1.23	0.615	**0.807**	0.616	0.665
Gd	5.70	6.24	3.95	3.04	3.30	3.71	1.42	**2.55**	1.73	1.84
Tb	0.776	0.881	0.588	0.440	0.444	0.462	0.252	**0.297**	0.215	0.209
Dy	4.29	4.84	3.25	2.45	2.17	2.25	1.52	**1.93**	1.02	0.97
Ho	0.907	0.900	0.667	0.484	0.432	0.450	0.335	**0.326**	0.223	0.220
Er	2.20	2.52	1.72	1.14	1.18	1.23	1.08	**0.961**	0.580	0.503
Tm	0.332	0.332	0.372	0.214	0.171	0.182	0.161	**0.146**	0.078	0.077
Yb	1.97	2.03	1.67	1.21	0.975	1.23	0.927	**0.738**	0.453	0.469
Lu	0.253	0.322	0.277	0.155	0.146	0.179	0.142	**0.121**	0.056	0.062
Hf	4.70	5.18	1.46	3.50	2.44	1.70	2.54	**3.66**	2.72	2.00
Ta	0.780	0.750	0.601	0.188	0.295	0.231	0.319	**0.429**	0.331	0.110
Pb	4.11	5.08	2.11	11.50	5.47	5.49	6.50	**2.08**	3.04	5.70
Th	3.18	3.60	2.66	2.47	3.72	3.19	4.31	**2.26**	2.53	1.96
U	0.534	0.610	0.480	0.334	0.438	0.422	1.03	**0.200**	0.093	0.430
$(La/Yb)_N$	10.79	10.91	6.79	9.65	15.78	11.91	7.79	**13.26**	19.97	20.58
$(La/Sm)_N$	3.04	2.84	2.47	2.62	3.22	2.91	3.60	**2.99**	4.71	4.35
$(Gd/Yb)_N$	2.34	2.48	1.91	2.03	2.74	2.44	1.24	**2.79**	3.09	3.17
Eu/Eu*	0.91	0.84	0.84	1.00	1.00	0.90	1.15	**0.88**	1.07	1.04

Table 1. (Contd.)

Component	*31*	*32*	*33*	*34*	***35***	*36*	***37***	*38*	*39*
	K-62/97	K-63/97	K-64/97	K-56/97	**K-79/97**	K-68B/97	**K-59/97**	K-60/97	K-61/97
SiO_2	67.40	65.59	70.63	74.50	**77.47**	77.09	**60.01**	69.52	69.64
TiO_2	0.42	0.53	0.39	0.22	**0.21**	0.23	**0.76**	0.39	0.33
Al_2O_3	17.49	16.62	16.02	14.44	**14.02**	14.86	**19.49**	15.41	16.25
Fe_2O_3	3.54	5.17	3.13	1.89	**1.57**	1.33	**5.91**	4.30	3.60
MnO	0.13	0.13	0.13	0.13	**0.12**	0.11	**0.15**	0.14	0.13
MgO	1.50	3.01	1.20	0.77	**1.31**	0.69	**1.93**	1.19	1.03
CaO	3.57	3.70	3.73	2.55	**1.50**	1.20	**6.07**	3.03	3.59
Na_2O	3.32	3.93	3.37	3.16	**0.46**	1.35	**3.66**	3.20	3.48
K_2O	2.51	1.17	1.29	2.27	**3.26**	3.08	**1.78**	2.69	1.85
P_2O_5	0.11	0.15	0.09	0.07	**0.06**	0.05	**0.23**	0.11	0.10
Li	7.32	16.9	9.7	9.60	**15.3**	17.8	**30.2**	37.3	27.9
Sc	7.33	10.8	6.43	2.86	**3.33**	3.82	**8.23**	7.40	5.70
Ti	2130	2446	1940	1010	**994**	1148	**3990**	2046	1680
V	55.8	51.7	45.0	17.0	**13.0**	14.6	**46.5**	32.1	41.7
Cr	41.3	52.8	35.5	29.3	**12.0**	32.0	**11.4**	27.5	40.0
Co	10.2	13.8	9.08	3.25	**2.46**	4.76	**12.2**	8.75	7.76
Ni	30.0	32.3	27.7	18.2	**12.7**	15.3	**10.1**	20.6	22.2
Cu	14.9	10.2	13.3	6.38	**5.79**	17.5	**1.57**	25.6	7.53
Zn	49.2	73.7	41.4	27.9	**66.8**	36.2	**56.3**	45.2	46.1
Ga	19.4	18.0	17.7	15.6	**17.1**	19.5	**19.4**	16.9	18.9
Rb	61.6	37.4	34.5	54.5	**86.8**	61.0	**42.8**	64.7	39.7
Sr	413	287	431	151	**136**	311	**487**	250	330
Y	4.71	8.19	4.50	6.35	**6.78**	8.76	**12.0**	19.3	11.0
Zr	99.0	107.0	95.0	103	**85.0**	104	**195**	121.0	91.0
Nb	3.82	3.91	1.89	8.3	**10.0**	11.7	**6.59**	8.59	4.40
Cs	1.90	1.55	1.02	2.21	**2.10**	1.26	**2.62**	1.79	2.81
Ba	490	320	411	497	**471**	400	**509**	623	462
La	12.8	20.6	12.3	30.0	**31.9**	32.0	**18.7**	24.3	17.7
Ce	25.0	31.9	23.5	61.8	**62.5**	66.5	**37.4**	45.0	32.6
Pr	2.93	4.94	2.77	6.65	**7.14**	7.08	**5.54**	7.25	4.26
Nd	12.00	17.90	10.90	22.40	**22.20**	24.13	**22.40**	25.80	16.44
Sm	2.08	3.00	2.05	3.19	**3.11**	3.72	**3.85**	4.84	2.71
Eu	0.774	0.899	0.602	0.71	**0.648**	0.714	**1.350**	0.979	0.782
Gd	1.65	2.73	1.53	2.51	**2.50**	2.50	**3.22**	3.57	2.48
Tb	0.225	0.293	0.207	0.317	**0.248**	0.328	**0.388**	0.540	0.332
Dy	1.00	1.42	0.96	1.22	**1.02**	1.44	**2.03**	2.98	1.81
Ho	0.182	0.311	0.190	0.219	**0.197**	0.261	**0.418**	0.605	0.371
Er	0.518	0.741	0.456	0.637	**0.597**	0.650	**1.35**	1.96	1.03
Tm	0.073	0.128	0.068	0.102	**0.074**	0.096	**0.209**	0.33	0.143
Yb	0.436	0.634	0.363	0.624	**0.445**	0.570	**1.34**	2.14	0.960
Lu	0.062	0.099	0.043	0.088	**0.061**	0.090	**0.21**	0.370	0.149
Hf	2.49	3.02	2.06	2.53	**2.63**	3.14	**2.02**	3.23	2.85
Ta	0.248	0.265	0.116	0.729	**0.697**	0.693	**0.431**	1.11	0.381
Pb	6.00	5.87	4.53	4.92	**10.90**	7.88	**4.32**	6.05	7.79
Th	2.40	3.82	1.94	8.13	**8.44**	8.85	**2.23**	5.76	3.35
U	0.506	0.592	0.409	1.66	**1.34**	2.91	**0.184**	1.09	0.751
$(La/Yb)_N$	19.82	21.93	22.87	32.45	**48.39**	37.87	**9.42**	7.66	12.48
$(La/Sm)_N$	3.87	4.32	3.78	5.92	**6.46**	5.41	**3.06**	3.16	4.12
$(Gd/Yb)_N$	3.06	3.48	3.41	3.25	**4.54**	3.55	**1.94**	1.35	2.09
Eu/Eu*	1.28	0.96	1.04	0.77	**0.71**	0.72	**1.17**	0.72	0.92

Note: (*1*, *2*) Tholeiitic metabasalts from the northern and southern parts of the structure (average of four); (*3*, *4*) metavolcanics of the boninite series; (*5*) Fe–Ti metabasalt (average of three). **Northern part of the structure:** (*6–8*) trondhjemites; (*9*) subvolcanic rhyodacite; (*10–14*) andesites 1; (*15–20*) andesites 2; (*21–22*) andesites. **Southern part of the structure:** (*23*) Nb–Ti andesites; (*24–29*) andesites and dacites; (*30–33*) subvolcanic rhyodacites; (*34–36*) subvolcanic rhyolites; (*37–39*) diorites and granodiorites. Printed in boldface are analyses of dated samples. Oxides are given in wt %, elements are in ppm, dashes mean not determined. All analyses are recalculated to anhydrous residue.

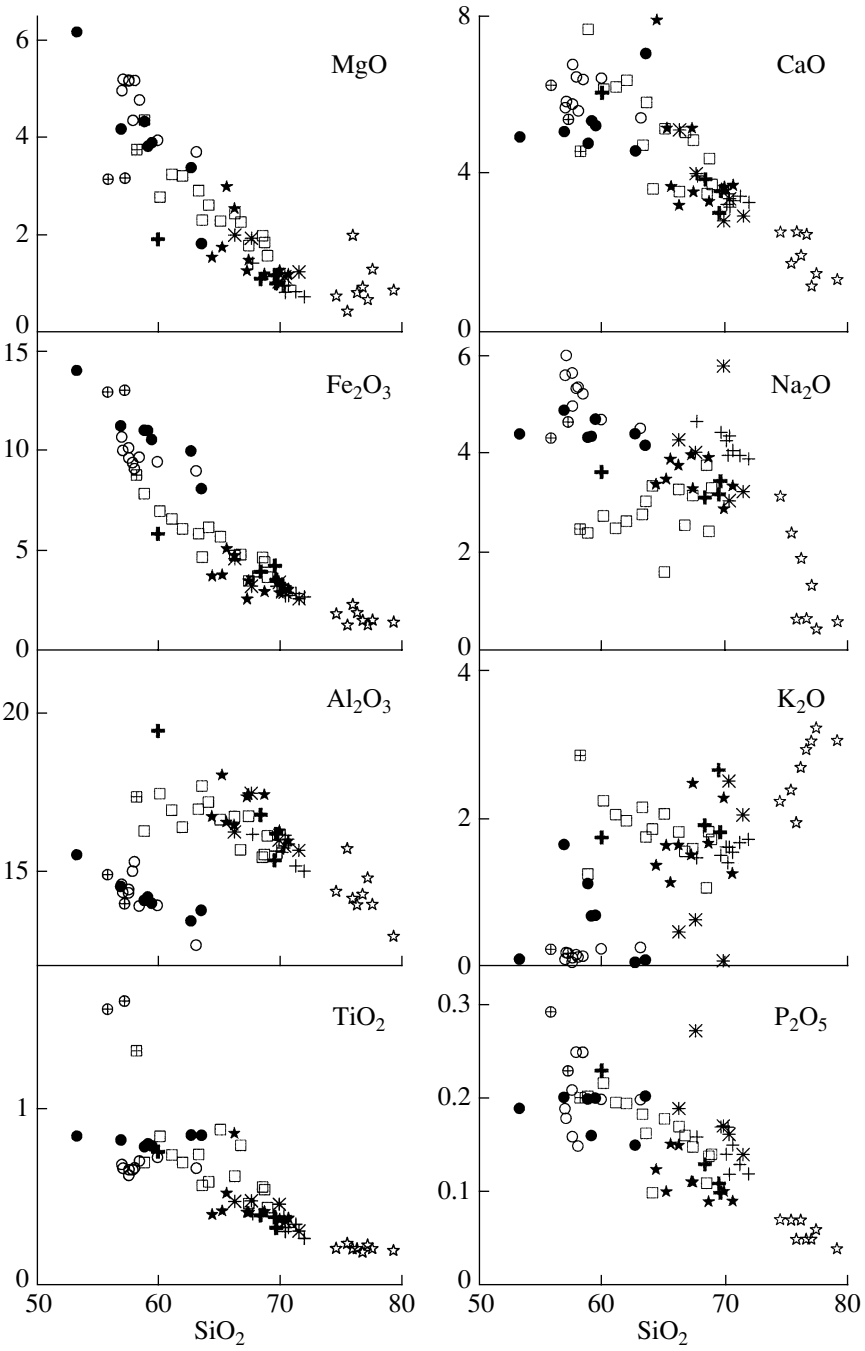

Fig. 6. Harker diagram (wt %) for major elements in intermediate and acid rocks of the Hisovaara structure. See Fig. 5 for symbol explanations.

4.5] and pervasively present Eu, Sr, and HFSE negative anomalies (Table 1, Figs. 5–7, 9).

The **granitoids framing the structure in the south** vary in composition from diorite to granodiorite and differ from the "northern" trondhjemites by higher concentrations of Nb, Y, and HREE, less fractionated LREE and, particularly, HREE patterns [$(La/Sm)_N$ = 3.2–4.1, $(Gd/Yb)_N$ = 1.3–2.1], and pervasive negative anomalies at Eu (Eu/Eu* = 0.72–0.95) and Ti (Table 1, Figs. 5–7, 9). One sample of diorite composition (SiO_2 = 60 wt %) was strongly enriched in Al_2O_3, CaO, Sr, and Eu (Eu/Eu* = 1.2), depleted in Zr, Cr, and Ni, and, perhaps, represents a part of the granitoid massif enriched in cumulus plagioclase. The significant variations in the LREE and HREE concentrations at close SiO_2 contents in the granodiorites (Figs. 7, 9) can be explained by the unequal distribution of accessory minerals concentrating REE.

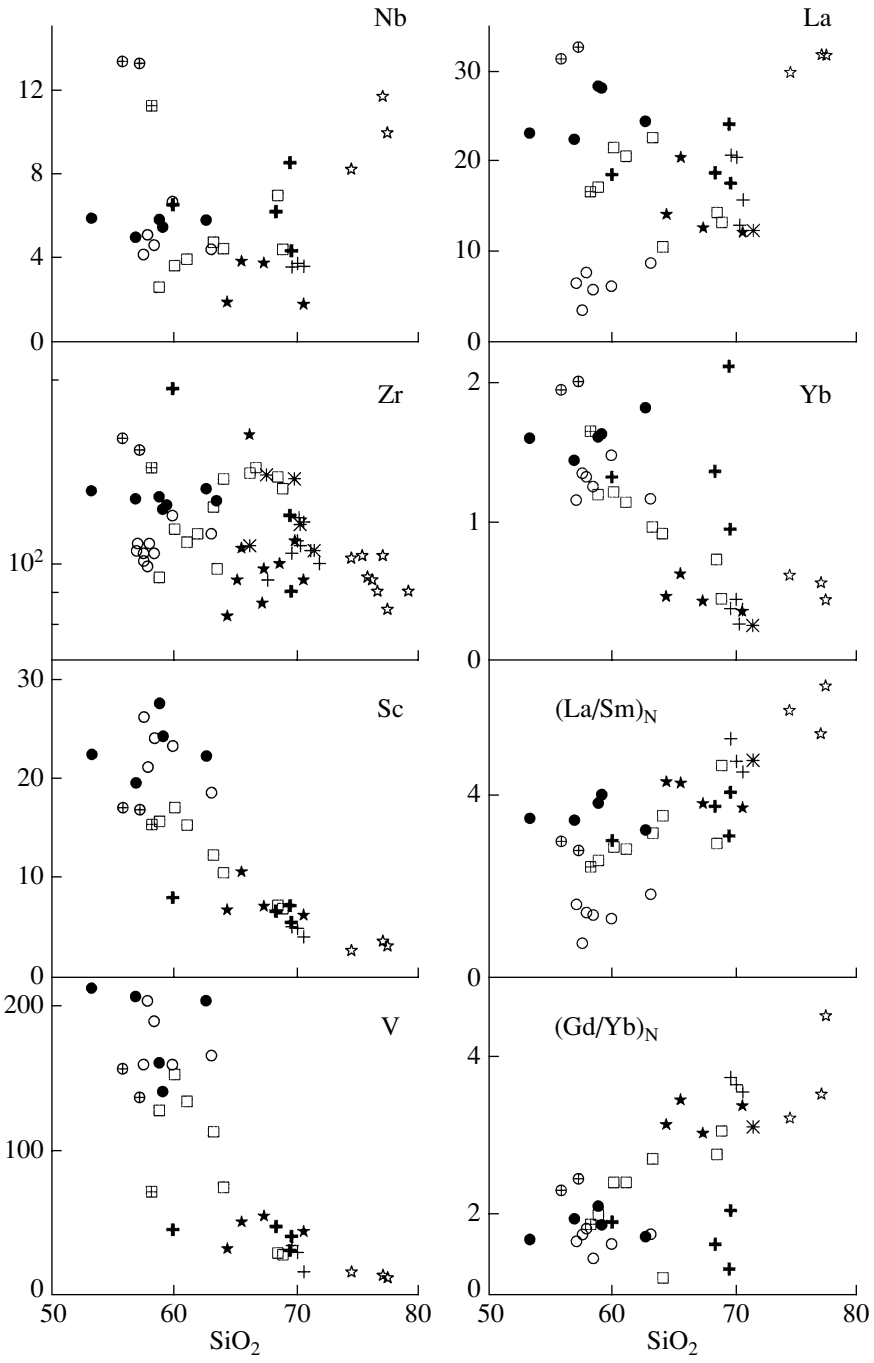

Fig. 7. Harker diagram (ppm) for trace elements in intermediate and acid rocks of the Hisovaara structure. See Fig. 5 for symbol explanations.

U–Pb ZIRCON DATING

The mineralogical study and U–Pb dating of the zircon were conducted on six samples of acid rocks from different parts of the structure: (1) medium-grained trondhjemite near the northern border (sample 15/96), (2) andesite 2 from the northern part of the structure (sample 7/96), (3) volcanic dacite from the southern portion of the structure (sample 76/97), (4) subvolcanic rhyolite from the southern portion of the structure (sample 79/97), (5) medium-grained diorite from the southern portion of the structure (sample 59/97), and (6) *Ms–Pl–Qtz* schist of terrigenous–sedimentary provenance from the central part of the structure (sample 10/96). The sampling sites of the rocks dated in this research are shown in the map (Fig. 2), and their petrochemical characteristics are listed in Table 1. The results of the U–Pb isotopic–geochemical study are

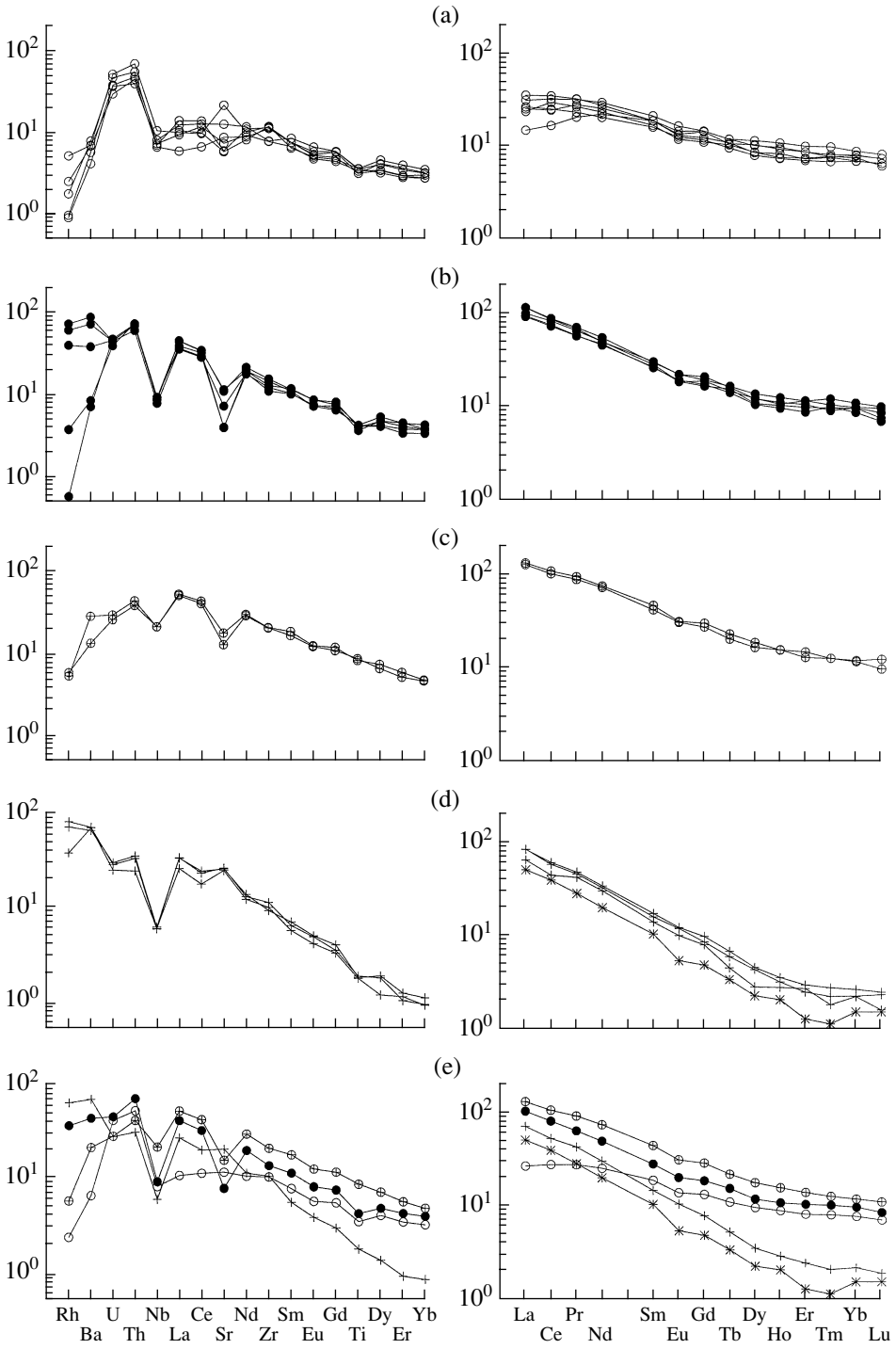

Fig. 8. Patterns of trace elements normalized to the primitive mantle (Hofmann *et al.*, 1988) and REE normalized to C1 chondrite (Evensen *et al.*, 1978) for intermediate and acid rocks in the northern part of the Hisovaara structure.

(a) Andesite 1; (b) andesite 2; (c) andesite 3; (d) surrounding trondhjemite and subvolcanic rhyodacite; (e) averaged patterns for the rocks (a)–(d).

summarized in Tables 2 and 3 and portrayed in Figs. 10a–10f.

Trondhjemite from the northern surroundings of the structure, sample 15/96. The accessory zircon of this rock consists of small (120 μm) euhedral prismatic grains, which are transparent, have a pale pinkish color, and bear single inclusions of other minerals and, rarely, older cores. The crystals have corroded faces and show no traces of newly formed overgrowths. The U concentrations are quite low, 120–140 ppm (Table 3). The

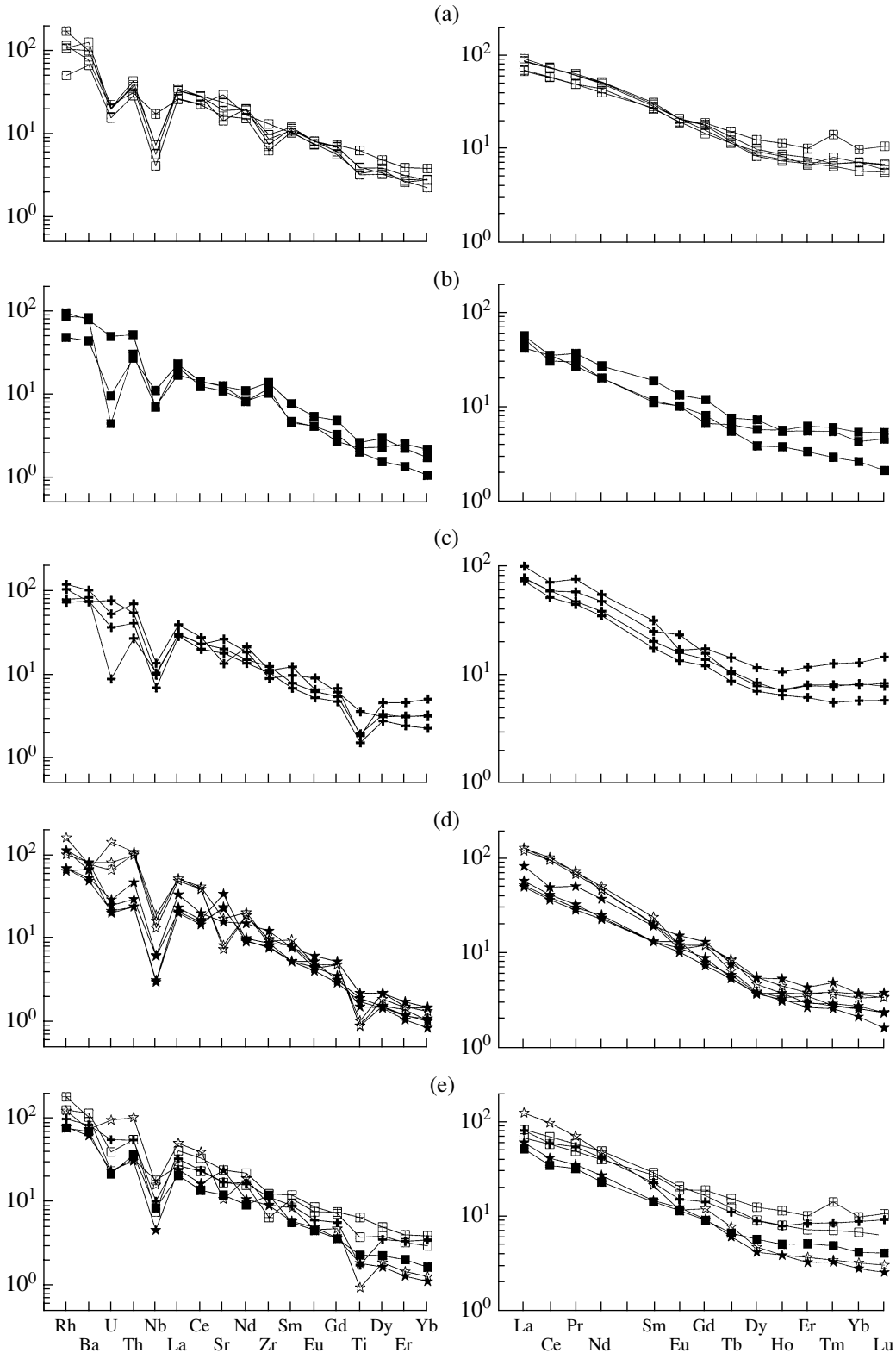

Fig. 9. Patterns of trace elements normalized to the primitive mantle (Hofmann *et al.*, 1988) and REE normalized to C1 chondrite (Evensen *et al.*, 1978) for intermediate and acid rocks in the southern part of the Hisovaara structure.

(a) Volcanic andesite; (b) volcanic dacite; (c) diorite and granodiorite at the southern surrounding; (d) subvolcanic rhyodacite and rhyolite; (e) averaged patterns for the rocks (a)–(d).

Table 2. U–Pb isotopic data on zircon from acid rocks of the Hisovaara structures and granitoids at its periphery

No.	Size fraction, μm	Sample, g	Concentration, ppm		Pb isotopic composition			Isotopic ratios and age, Ma		
			U	Pb	$^{206}Pb/^{204}Pb$	$^{206}Pb/^{207}Pb$	$^{206}Pb/^{208}Pb$	$^{206}Pb/^{238}U$	$^{207}Pb/^{235}U$	$^{207}Pb/^{206}Pb$
K-76/97, dacite										
1	–60 + 45	0.0032	102.07	44.60	12050	6.014	9.273	0.3994	9.108	2511.3 ± 2
2	–75 + 60	0.0021	234.03	113.33	12200	5.728	8.525	0.4359	10.439	2593.7 ± 2
3	–125 + 100	0.0013	62.94	31.47	4525	5.4696	8.267	0.4488	11.155	2655.4 ± 2
4	–45 SL	0.0031			1250	4.904	5.789	0.5383	14.434	2780.3 ± 3
								2776.4	2778.7	
5	–75 + 60 SL	0.0082			4445	5.115	6.862	0.5349	14.232	2767.5 ± 2
								2762	2765.3	
K-79/97, rhyolite										
1	+100	0.0027	514.42	285.0	3550	5.344	6.546	0.4786	12.133	2687.8 ± 4
2	–75 + 60	0.0017	553.17	300.25	6000	5.403	6.332	0.4687	11.840	2682.1 ± 2
3	–60 SL	0.001			1380	4.9933	5.4749	0.5160	13.6385	2756.9 ± 3
4	–60 SL	0.001			1750	5.0625	1.5126	0.5099	13.4166	2749.2 ± 2.6
5	–100, abraded	0.00038	661.76	365.61	3390	5.3294	6.2077	0.4754	12.073	2691.1 ± 2.1
6	–100, abraded	0.0011	618.35	344.51	4350	5.356	6.303	0.4799	12.183	2690.0 ± 2
7	+100, abraded	0.0007	607.5	342.69	5750	5.346	6.6181	0.4894	12.490	2699 ± 1.9
Kh-15/96										
1	+100	0.0043	138.03	77.49	830	4.866	6.853	0.4804	12.663	2752.4 ± 4.5
2	–100 + 90	0.0012	124.16	64.10	8100	5.253	9.587	0.4651	12.123	2733.9 ± 1.9
3	–90 + 60	0.0025	128.69	67.404	4020	5.220	8.588	0.4692	12.209	2731.1 ± 2
4	+60 SL	0.0023	141.58	72.95	4290	5.239	9.159	0.4603	11.946	2726.7 ± 2
5	–45	0.0006	120.61	60.99	870	5.053	6.326	0.4391	11.1468	2690.1 ± 4.3
6	–45 SL	0.007			2100	5.323	8.697	0.4168	10.473	2673.2 ± 2.5
Kh-10/96										
1	+125	0.00035	296.29	154.6	900	5.151	5.044	0.4324	10.779	2660.2 ± 4.3
2	–100 + 90	0.0012	265.94	132.43	1330	5.431	5.628	0.4215	10.175	2606.8 ± 3.3
3	–75 + 60	0.0008	364.21	171.81	1920	5.602	5.974	0.4056	9.633	2579.7 ± 2.7
4	+45	0.0007	538.49	272.71	410	4.950	4.266	0.4028	9.565	2579.5 ± 9.3
K-59/97, tonalite										
1	+100	0.002	113.79	65.08	10750	5.119	8.825	0.5089	13.638	2779.5 ± 1.9
2	–100 + 75	0.0009	118.92	71.24	1700	4.956	6.805	0.5159	13.863	2783.7 ± 2.6
3	–75 + 60	0.0022	123.30	71.09	9170	5.099	8.165	0.5088	13.675	2784.3 ± 1.9
4	–60	0.001	146.13	80.02	6200	5.192	8.382	0.4868	12.807	2749.3 ± 1.9
5	SL	0.0065			4280	5.087	8.416	0.4798	12.828	2775.7 ± 2.0

Note: SL—after selective leaching; the U and Pb concentrations were not determined because of the sample uncertainty.

morphology of the zircon and its geochemistry testify to its magmatic genesis. The isotopic ages are discordant. Our efforts to increase the concordancy by air abrasion and selective leaching did not yield positive results. The data point of the zircon fraction after selective acid treatment was shifted downward and to the right in the concordia plot (Fig. 10a), a fact suggesting the presence of a somewhat older, strongly disturbed component in crystal cores. The age defined by the discordia (the SL fraction was excluded) was 2804 ± 27 Ma.

Andesite 2 from the northern part of the structure, sample 7/96. We managed to obtain as few as approximately 20 zircon grains from a large 10-kg andesite sample. The grains were small (<70 μm),

Table 3. U–Pb isotopic data on zircon from metaandesite (sample 7/96) of the Hisovaara structures (NORD-SIM)

Grain number	$^{206}Pb/^{204}Pb$ measured	Concentration, ppm			$^{207}Pb/^{206}Pb$ isotopic age	Isotopic ratios		Discordance, %
		Pb	U	Th		$^{206}Pb/^{238}U$	$^{207}Pb/^{235}U$	
06a	10500	81	117	56	2762	0.5268	13.9672	1.5
06b	21000	99	140	62	2777	0.5369	14.3610	0.3
08a	24000	109	147	131	2769	0.5191	13.8189	3.2
08b	52000	112	149	124	2748	0.5268	13.8465	0.9
09a	48000	205	257	261	2740	0.5509	14.4062	+4
11a	100310	137	176	156	2748	0.5557	14.6072	+4.6
13a	17220	88	227	119	2751	0.2830	7.4859	–46.6

euhedral, prismatic, with lustrous faces without traces of dissolution. Judging from their optical characteristics, the zircon crystals are homogeneous, transparent, nearly colorless, finely zoned, sometimes with small (<10 μm) strongly resorbed inclusions of older zircon and microincluions of foreign minerals. It is hard to reliably identify the nature of the zircon because of the limited amount of the material. The good preservation of crystal surfaces suggests the absence of overprinted processes, which, in turn, points to a metamorphic (rather than magmatic) genesis of the zircon. Inclusions visible in these crystals can, thus, be ascribed to relict protolithic, premetamorphic zircon. Homogeneous zircon grains were analyzed on a NORDSIM ion microprobe in Stockholm. The results are listed in Table 3 and shown in a concordia plot (Fig. 10b). The elevated U concentrations (up to 260 ppm) in some of the zircon grains are generally atypical of magmatic zircon in andesites and furnish additional evidence for the metamorphic genesis of this mineral. The isotopic ages are highly concordant. The most concordant zircon grain yielded an isotopic age of 2777 ± 5 Ma (Table 3). The age determined by the upper intercept between the discordia and concordia (at the lower-intercept age fixed at 1750 Ma) is 2783 ± 36 Ma (Fig. 10b). The value of 1750 Ma corresponds to the most probable disturbance timing of the U–Pb system of the zircon due to metamorphism related to the Lapland collision (Bibikova *et al.*, 1999b). Hence, the age of 2777 ± 5 Ma seems to correspond to the crystallization time of the zircon, and, taking into account its probable metamorphic genesis, the timing of the earliest metamorphic recycling of volcanogenic rocks in the northern part of the Hisovaara structure. Inclusions of an earlier zircon generation, which could be zircon from the magmatic protolith of the metaandesites, were not dated because of the small sizes of their grains.

Volcanic dacite from the southern part of the structure, sample 76/97. The accessory zircon occurs as small (120 μm) euhedral prismatic crystals, which have an elongation of 2–3.5 and are transparent and pale pinkish in color. The internal structure of the crystals is homogeneous, there is often fine concentric zoning, inclusions of foreign phases are rare, and there seems to be no older zircon cores of older generation. The faces of the crystals exhibit etching traces, no newly formed zircon overgrowths were noticed. All of these features testify to the magmatic genesis of the zircon. The isotopic ages of the untreated fractions are discordant, but acid leaching resulted in the removal of the U-richest zircon phase and a concordant age. The age of the concordant zircon fraction is 2780 ± 21 Ma (Fig. 10c) and corresponds to the timing of dacite volcanism in the southern part of the structure.

Subvolcanic rhyolite from the southern part of the structure, sample 79/97. Zircon occurs in this rocks in the form of euhedral prismatic crystals with an elongation of 2–4. Zircon crystals are semitransparent, nearly colorless, and bear numerous inclusions of ore minerals. No older zircon cores were detected, neither was identified an inherited zircon component in the zircon fractions after abrasion and acid leaching (Table 2). The U concentration of the zircon is relatively high, 500–600 ppm, as is characteristic of magmatic zircon in similar rocks. The isotopic ages are discordant. The upper intercept between the discordia and concordia corresponds to an age of 2796 ± 15 Ma (Fig. 10d) and is interpreted as the intrusion timing of the subvolcanic rhyolites.

Medium-grained diorite gneiss near the southern border of the structure, sample 59/97. The accessory zircon from this rock is comprised of large subprismatic grains with rounded vertexes, semitransparent, and strongly fractured. Several grains contain inner cores. The U concentrations are relatively low, 100–150 ppm, and the isotopic ages are strongly discordant. When one of the fractions was selectively leached to remove the most disturbed phase, the degree of concordancy of this fraction did not increase, but the data point appeared to be shifted to the right from the discordia toward older ages, a fact suggesting that the zircon cores contained an older but strongly discordant phase. The age corresponding to the upper discordia and concordia intercept (without the SL fraction) is 2826 ± 18 Ma (Fig. 10e).

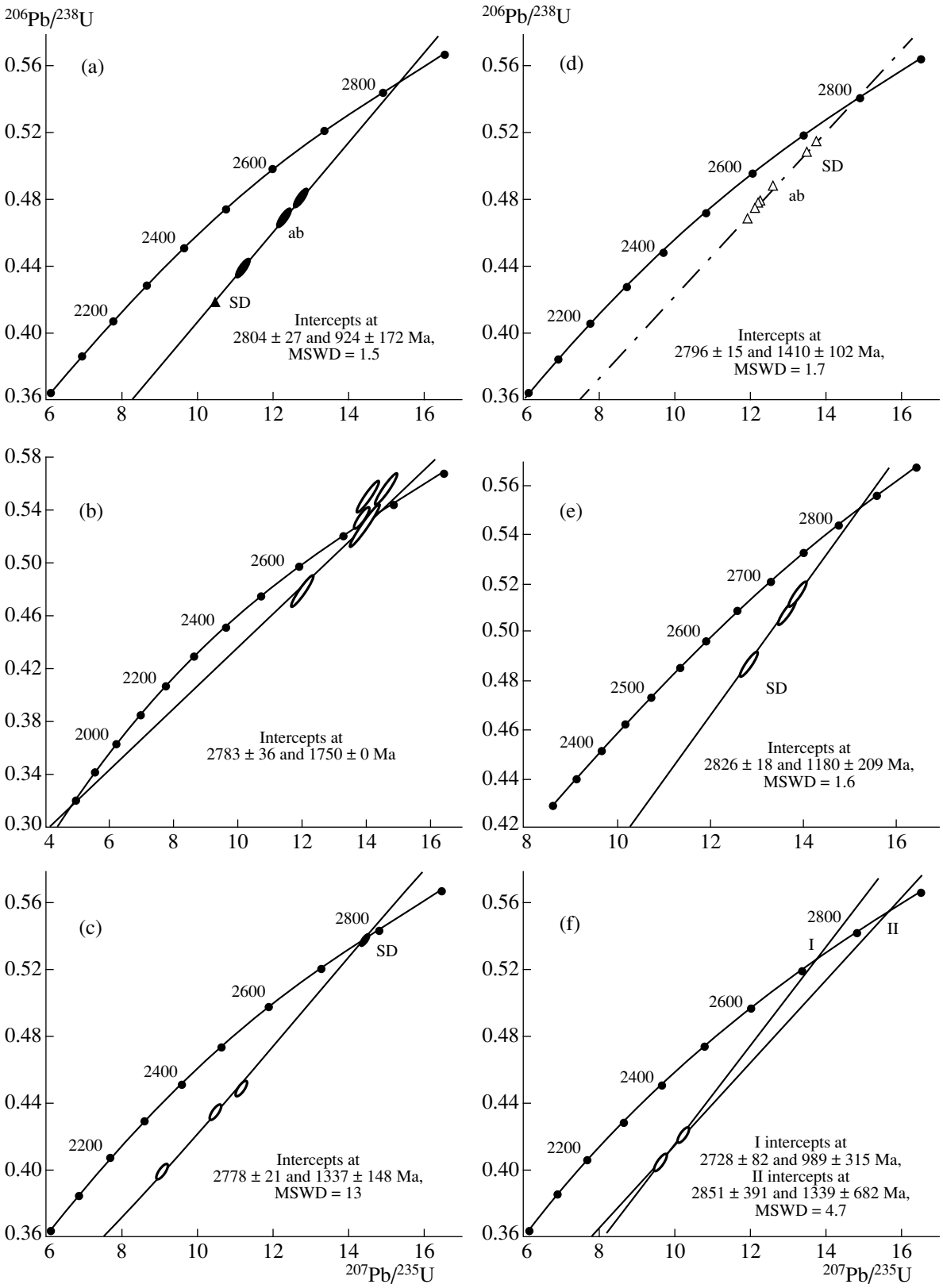

Fig. 10. Concordia diagram for zircon.

(a) Trondhjemite from the northern surrounding (sample 15/96); (b) andesite 2 from the northern part of the structure (sample 7/96); (c) dacite from the southern part of the structure (sample 76/97); (d) subvolcanic rhyolite from the southern part of the structure (sample 79/97); (e) diorite from the southern surrounding of the structure (sample 59/97); (f) metasedimentary *Ms–Qtz–Pl* schist from the central part of the structure (sample 10/96).

***Ms–Pl–Qtz* schist of terrigenous–sedimentary provenance from the central portion of the structure, sample 10/96.** The zircon fraction is strongly heterogeneous in terms of both the morphology and the optical properties of crystals. The fraction is dominated by variably sized (from 45 to 120 μm), prismatic to equant subhedral grains, strongly corroded, variably fractured, colorless to pale brown, with a homogeneous or finely zoned inner structure and different amounts of foreign inclusions. According to their morphology and optical characteristics, some of these zircons are close to zircon from the subvolcanic rhyolites in the southern limb. The strong reworking of the crystals was caused by either their mechanical transportation or dissolution in the course of metasomatic processes. Less common larger (90–150 μm) euhedral prismatic to long-prismatic crystals have a hyacinth habit, well preserved grains, are colorless, transparent, and carry abundant inclusions of foreign mineral phases, which resemble zircon from kyanite quartzites. The U concentrations in individual size fractions vary within a broad range, from 550 to 250 ppm, as a function of the geochemical heterogeneity of the zircon. The isotopic ages are strongly discordant, particularly for the fine-grained high-U fraction. The calculation with the use of all zircon fractions determines an age of 2851 ± 391 Ma for the intercept between the discordia and concordia. If the largest zircon fraction (which is usually the highest in relict cores) is rejected from the consideration, the age corresponding to the upper discordia–concordia intercept is 2728 ± 82 Ma. The large error seems to be caused by both the heterogeneity of the zircon and the closely spaced arrangement of the data points (the lack of their spread along the discordia) in the plot (Fig. 10f). The inspection of zircon from the *Ms–Pl–Qtz* schists confirms the terrigenous–sedimentary nature of their protolith. The sediments were derived by the destruction of sources of various ages and with different geochemical characteristics, with the leading contribution made by a proximal source, perhaps, the acid volcanics in the southern part of the structure. Along with them, a distal source of terrigenous material is probable, which possibly included some more ancient rock complexes than those exposed at the surface.

DISCUSSION

Petrogenetic and Tectonic Nature of the Intermediate and Acid Rocks of the Hisovaara Structure

Our results indicate that the intermediate and acid rocks of the Hisovaara structure comprise three distinct groups, which could be produced in different tectonic regimes.

The andesites in the northern part of the structure are petrochemically close to tholeiitic andesites of Phanerozoic and modern initial intracontinental island arcs (Baker, 1982, and references therein; Meijer *et al.*, 1982; Staudigel *et al.*, 1999). This analogy is also emphasized by the similarities between the rock associations, because, as in Phanerozoic arc complexes (Meijer *et al.*, 1982; Staudigel *et al.*, 1999), the tholeiitic andesites of the northern part of the Hisovaara structure are closely associated with low-Ti tholeiites, volcanics of the boninite series, and Fe–Ti basalts (Shchipansky *et al.*, 1999, 2002). However, compared with Phanerozoic analogues the tholeiitic andesites of the Hisovaara structure have more fractionated REE patterns depleted in HREE (Figs. 11a, 11b) and lower concentrations of Sc and Y. This fact implies that, in contrast to Phanerozoic tholeiitic andesites, whose genesis is thought to be related to the shallow-depth (olivine + amphibole + pyroxene + plagioclase) differentiation of tholeiitic basalts (Baker, 1982), the petrogenesis of the Hisovaara andesites was participated by a mineral phase with a high Kd for Yb, Y, and, perhaps, Sc, which could be garnet. Indeed, geochemical simulation indicates that andesites 1 and 3 could be produced by the differentiation of, respectively, tholeiitic and Fe–Ti basalts in the presence of 10% garnet in the cumulus assemblage (Table 1, Figs. 12a–12c), which implies relatively deep (no less than 15 kbar) differentiation conditions (Stern *et al.*, 1975). The derivation of the parental melts for andesites 2 cannot be explained by the crystallization differentiation of any basalts of the Hisovaara structure or andesites 1. In the latter situation, LREE enrichment could be attained only at very profound (90%) differentiation (Fig. 12b), which is improbable given similarities between most petrogeochemical characteristics of andesites 1 and 2. An alternative explanation can rely on the supposed origin of andesites 2 by the addition of LREE to andesites 1, with LREE derived from a source with high concentrations and strongly fractionated patterns of these elements. These could be sedimentary rocks brought to the magma generation region with a subducting plate.

The subvolcanic dacites, rhyodacites, and rhyolites in the northern and southern parts of the structure and the trondhjemites framing it in the north show similar petrochemical features and are analogous to Phanerozoic adakites (Fig. 13), which are believed to have been derived by the partial melting of metamorphosed basalts of the subducted oceanic plate (Drummond and Defant, 1990; Rapp *et al.*, 1991; Rapp and Watson, 1995; Martin, 1999). This is consistent with the results of REE simulations, according to which these rocks could be derived by the partial melting of metabasites (with geochemical characteristics similar to those of tholeiitic basalts in the northern part of the structure) in equilibrium with an amphibole–garnet–plagioclase–clinopyroxene residue (Fig. 12d). The high-Al rhyolites of this series could be produced by the 40% crystallization differentiation of the subvolcanic rhyodacites with the fractionation of the assemblage of plagioclase (50%) + hornblende (25%) + quartz (20%) + ilmenite (5%) (Fig. 12e). A similar mineralogic composition of the residue was obtained experimentally by 40–50% melting of rhyodacite with

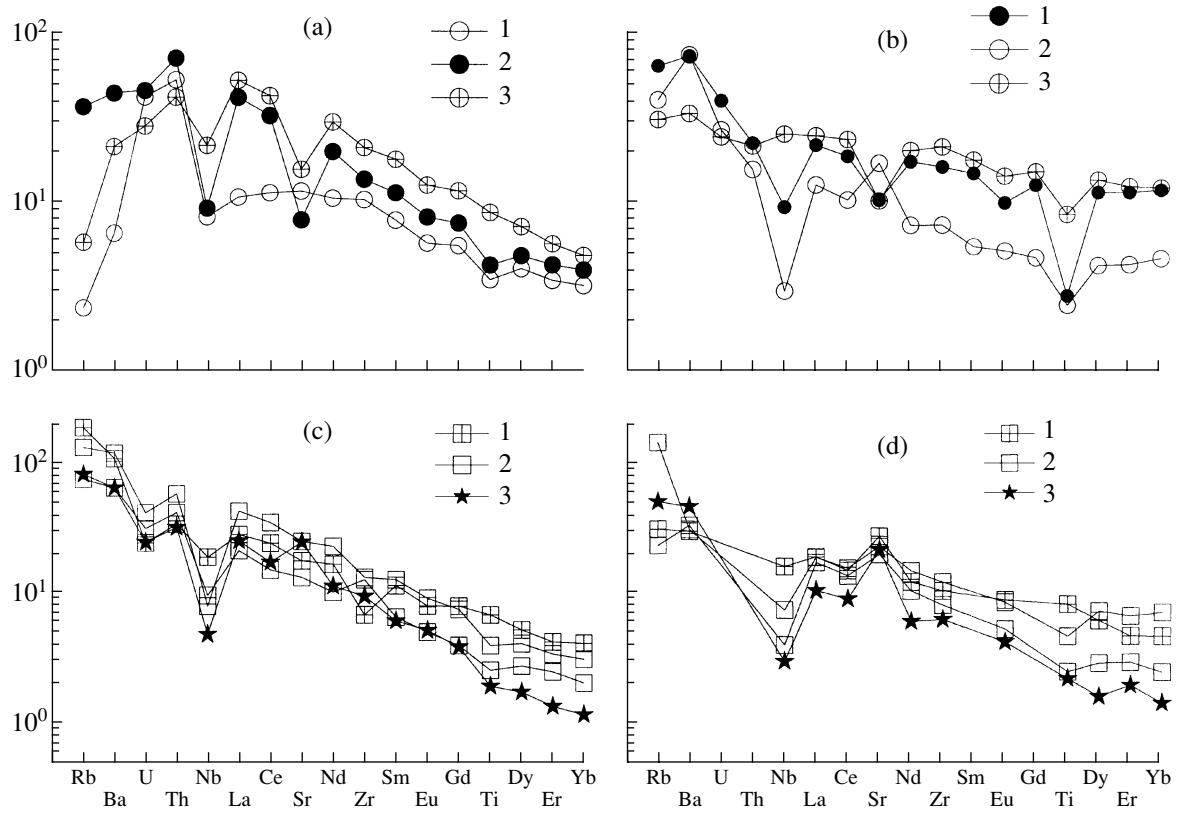

Fig. 11. Patterns of trace elements normalized to the primitive mantle (Hofmann *et al.*, 1988) for intermediate and acid rocks of the Hisovaara structure and Phanerozoic island-arc complexes.

(a) Andesite 1 (1), andesite 2 (2), and andesite 3 (3) from the northern part of the Hisovaara structure; (b) tholeiitic low-Ti andesites with (1) the minimum and (2) maximum REE concentrations from the Mariana Trench (Lin *et al.*, 1989; Peate *et al.*, 1998) and (3) produced in an back-arc spreading environment in the East Scotia Ridge (Leat *et al.*, 2000); (c) Nb–Ti andesite (1), calc–alkaline andesites and dacites (2) and subvolcanic dacites–adakites (3) from the southern part of the Hisovaara structure; (d) Nb–Ti andesites (1), calc–alkaline andesites and adakites (2), and adakites (3) from Mindanao Island, Philippines (Sajona *et al.*, 1994).

the derivation of a highly silicic melt under pressures of 0.2–1.0 kbar at 4–9 wt % water in the system (Prouteau *et al.*, 1999). The compositional gap between the rhyodacites and rhyolites over the interval of 70–74 wt % SiO_2 can be explained by the poor representativeness of the sampling but could also be caused by the transportation of the melt by discrete portions from shallow-depth intermediate chambers. In contrast to most Phanerozoic adakites, related to the subduction of relatively thin hot plates, Archean adakites as a whole and our adakites among others have lower Mg# and are less enriched in Fe-group elements, a fact pointing to insignificant interaction between the melts derived from the plate and the overlying mantle wedge (Martin, 1999). This, in turn, implies a relatively small thickness of the wedge, perhaps, because of a gentler subduction angle, which could be related to a greater thickness of the Archean crust due to elevated thermal regimes in the Archean mantle (Sleep and Windley, 1982).

The high-Al K–Na calc–alkaline andesites and dacites in the southern portion of the structure differ from classic BADR series in Phanerozoic island arcs. First, among the volcanics in the southern part of the Hisovaara structure no calc–alkaline basalts were found that could be regarded as parental melts derived by the partial melting of the metasomatically recycled mantle wedge. Second, the changes in geochemical characteristics with the transition from the Hisovaara andesites to dacites, for example, a decrease in the overall level of concentrations of LREE and HREE at an increase in the La/Yb ratio (Figs. 7, 9) are atypical of BADR series, they cannot be related to the fractionation of the cumulus association plagioclase + pyroxene + hornblende (typical of these series) and can be explained only by the removal of a phase (such as allanite) with a very high partition coefficient for LREE (Fig. 12f). At the same time, the close spatiotemporal association of the calc-alkaline andesites and dacites with Nb–Ti andesites and adakites is analogous to associations of island arcs where either a young hot or a thickened oceanic plate is subducted (Figs. 11c, 11d). The genesis of normal and Nb–Ti andesites is related to the partial melting of ultramafic rocks in the mantle wedge that had been recycled by the fluid constituent and adakite melts separated from the subducting plate (Drummond and Defant, 1990; Drum-

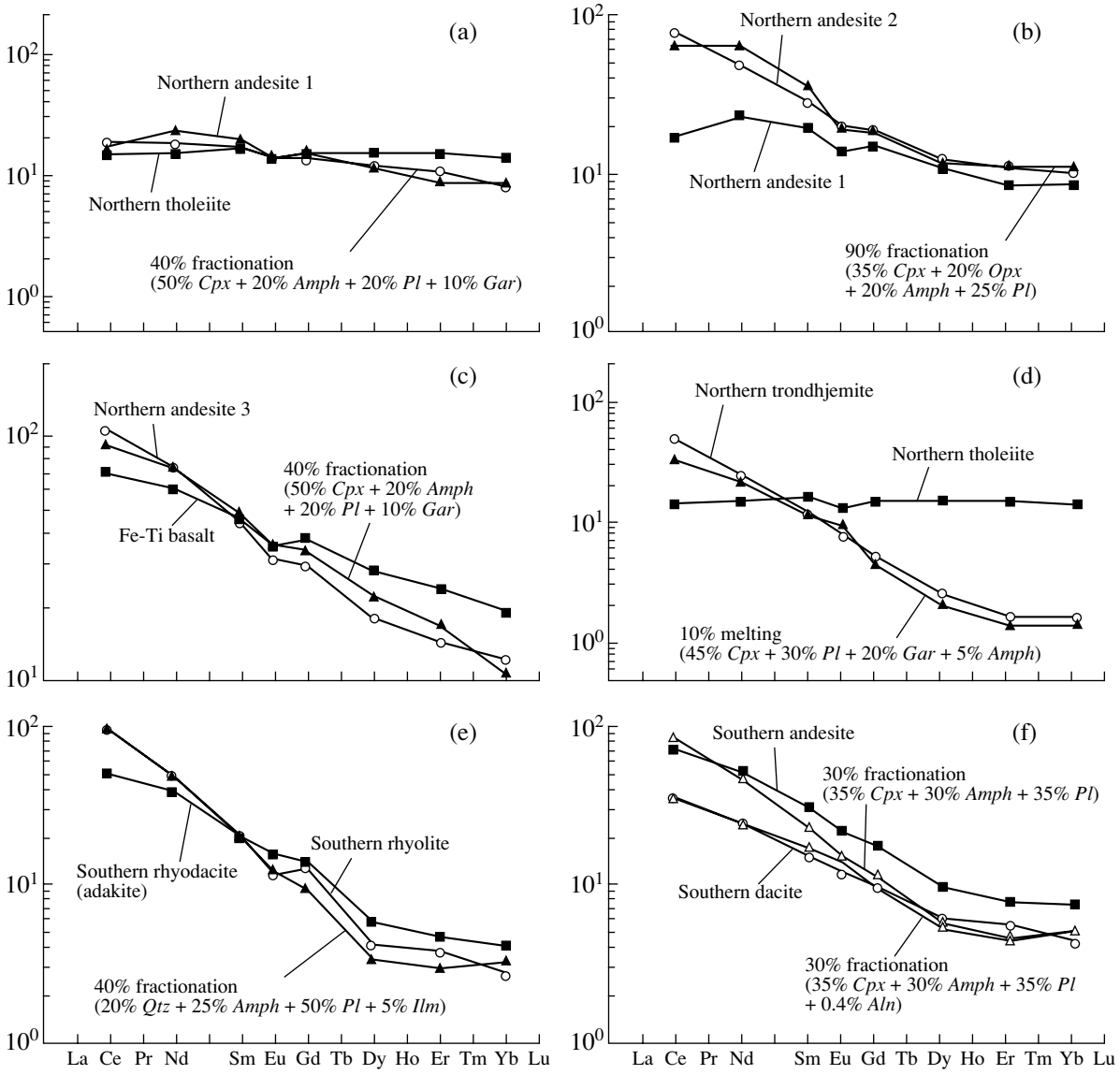

Fig. 12. C1 chondrite (Evensen *et al.*, 1978) normalized REE patterns for intermediate and acid rocks of the Hisovaara structure and model melts.

(a) Genesis of andesite 1 by the crystallization differentiation of tholeiitic basalt; (b) origin of andesite 2 by the differentiation of andesite 1; (c) origin of andesite 3 by the differentiation of Fe–Ti basalt; (d) partial melting of tholeiitic basalt with the origin of adakite melt; (e) crystallization differentiation of adakitic dacite with the origin of adakitic rhyolite; (f) differentiation in the succession calc–alkaline andesite–dacite from the southern part of the structure.

mond *et al.*, 1996; Sajona *et al.*, 2000; Proteau *et al.*, 2000). The changes in the petrochemistry of the calc–alkaline volcanics with the transition from andesites to dacites could be caused not only by differentiation but also by the addition of adakite melts either at shallow depths or at those where the calc–alkaline magmas were derived. This is also evident from the overlap of the compositions of the dacite volcanics and the subvolcanic adakite dacites in most binary diagrams (Figs. 6, 7, 9, 13). On the one hand, possible mixing between the calc–alkaline and adakite melts in shallow-depth intermediate chambers or during their eruption is pointed at by the fact that the dacite volcanics contain a bed of agglomerate rocks whose fragments have "adakitic" signatures (Kozhevnikov, 2000). On the other hand, the associations in the southern part of the Hisovaara structure exhibit obvious similarities with the products of Cayambe volcano in Ecuador (Samaniego *et al.*, 2002), whose calc–alkaline volcanism (0.5–0.25 Ma) gave way to eruptions of melts with geochemical signatures transitional to adakitic and adakite itself (<0.165 Ma) over a time period of less than 0.1 m.y. (Fig. 11b). This was supposedly related to the increased contribution of the adakite component to the mantle source during the passage of the thickened oceanic crust of the Carnegie Ridge through the subduction zone.

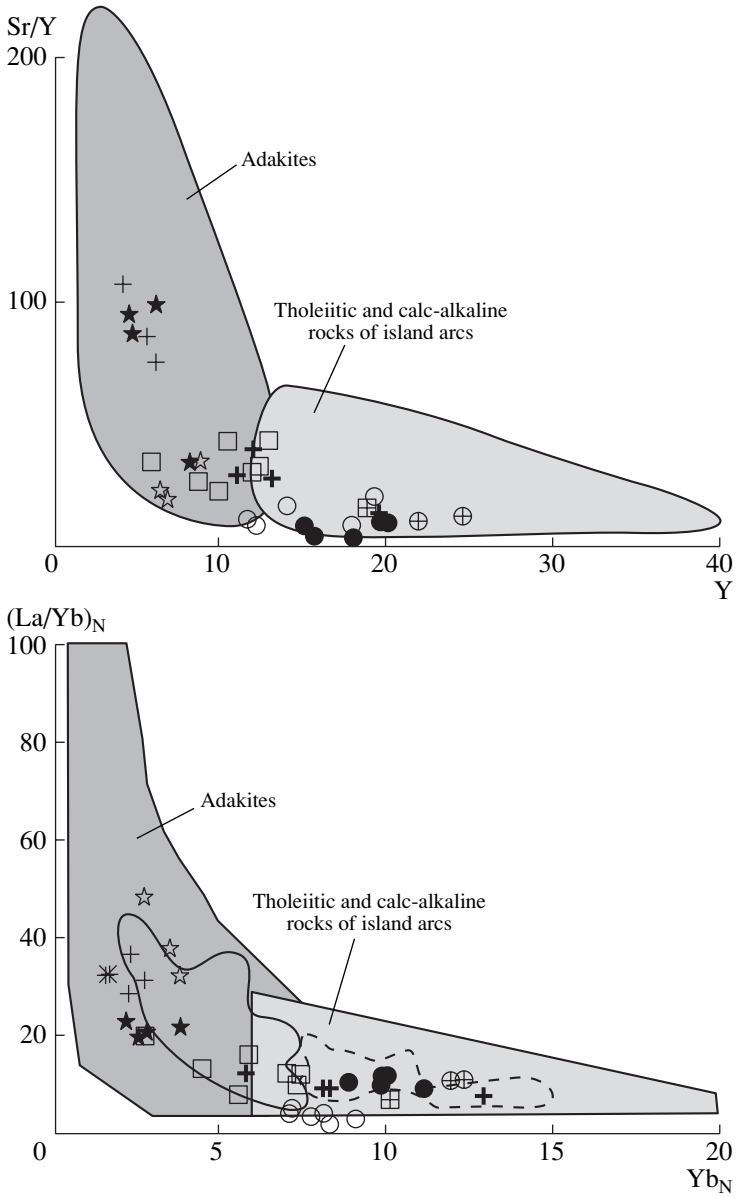

Fig. 13. $(La/Yb)_N$ vs. Yb_N and Sr/Y vs. Y diagrams for intermediate and acid rocks of the Hisovaara structure.

The fields of island-arc volcanics and adakites are given after (Martin, 1999). See Fig. 5 for symbol explanations. For comparison, the diagram also shows the fields of intermediate and acid volcanics of the calc–alkaline (dashed contour) and adakitic (solid-line contour) series of Cayambe volcano, Ecuador (Samaniego *et al.*, 2002).

The granodiorites framing the structure in the south show petrochemical similarities with the andesites and dacites in the southern part of the structure, which suggests the possibly comagmatic character of these rocks. However, this concept calls for a specialized study, given the tectonic (but not intrusive) character of relations between the southern-framing granitoids and the supracrustal rocks of the structure itself.

Age Relations

The petrological and tectonic reconstructions discussed both in this paper and elsewhere (Shchipansky *et al.*, 1999, 2002) point to the existence of two tectono–stratigraphic rock complexes of the Hisovaara structure, which were produced in different tectonic environments and, perhaps, at different times.

The first of them, the oldest complex comprises tholeiitic metavolcanics of mafic and intermediate composition in the northern part of the structure and, perhaps, also metabasites framing it in the south. The relatively old age of this complex follows from: (1) geologic relations between the mafic metavolcanics and trondhjemites framing the structure in the north, subvolcanic dacites, rhyodacites, and rhyolites in both the northern and the southern portion of the structure;

(2) petrogenetic relations between the mafic and intermediate rocks in the northern part of the structure; and (3) data on the earliest deformation event D1 whose traces were identified in the metavolcanics of the northern part of the structure (Kozhevnikov, 1992, 2000). The U–Pb isotopic geochronologic study of zircon from the andesites of this complex yielded an age of 2780 ± 10 Ma, which was interpreted as the timing of the oldest metamorphic episode, synchronous with the origin of the magmatic protoliths of the second, younger complex of the Hisovaara structure.

The second complex includes petrogenetically diverse calc–alkaline intermediate and acid volcanics in the southern portion of the structure, intrusive rocks of the adakite series, including subvolcanic dacites, rhyodacites, rhyolites, and trondhjemites framing the structure in the north, and, perhaps, also granodiorites near its southern margin and metasediments in its central part.

The close spatial association of the processes that gave rise to the magmatic protoliths of the intermediate and acid rocks and the subvolcanic facies of this complex, as is implied by geological and petrological evidence, is corroborated by the close U–Pb zircon ages of these rocks within the range of 2778 ± 21 to 2826 ± 18 Ma. The most reliable age value is determined by the concordant point for zircon (2780 ± 10 Ma) from metadacite in the southern part of the Hisovaara structure. Similar, within the error, age values were obtained for the upper intercepts between the discordias and concordia for subvolcanic rhyolites from the southern part of the structure (2796 ± 15 Ma) and framing trondhjemites in the north (2804 ± 27 Ma). The somewhat older U–Pb age of the latter could be caused by a slight turn of the discordia owing to the presence of an older zircon component in the magmatic zircon. An older, outside the error, age was obtained only for a magmatic zircon generation from the granitoids framing structure in the south (2826 ± 18 Ma), which could be caused by two factors. On the one hand, the diorite–granodiorite massif near the southern margin of the structure could be older than the rest of the volcanic and plutonic rocks of the Hisovaara structure, because geological–structural data do not suggest intrusive relations between these granitoids and the volcanic associations of the structure. On the other hand, given petrologic evidence of the intrusive emplacement of these granitoids and their geochemical similarities with the volcanics in the southern part of the Hisovaara structure, it seems to be more probable that the age values inferred from the discordia and concordia intercept was slightly overestimated due to the fact that this magmatic zircon population includes single grains or cores of older zircon that were either inherited from the source or entrapped during the melt evolution. A significant contribution of the latter is implied by both mineralogical results and isotopic–geochemical data on zircon samples after acid leaching.

The metamorphosed sedimentary rocks in the central part of the structure are, judging from mineralogical data on their zircon and geochemical evidence (Thurston and Kozhevnikov, 2000; author's unpublished data), of proximal character, with the material provided mostly by neighboring acid volcanics and quartz–kyanite rocks in the southern portion of the structure. This suggests the existence of temporal relations between acid volcanism in the southern portion of the structure and the accumulation of sediments, produced by either the destruction of preexisting volcanic centers or the redeposition of acid volcanic products. Conversely, weathering crust on the "northern" andesites underlying the metasedimentary quartzites (Thurston and Kozhevnikov, 2000) suggest the possibility of an age gap between the volcanic processes in the northern part of the structure and sedimentation in its central portion.

A Model for the Geodynamic Evolution of the Hisovaara Structure

Available data indicate that the two distinguished tectono–stratigraphic complexes correspond to two stages of the Archean evolution of the Hisovaara structure, which can, perhaps, be paralleled with the successive evolution of a single island arc.

During **the first stage,** tholeiitic volcanic of mafic and intermediate composition were produced in the northern part of the structure, possibly, along with tholeiitic basalts in its southern portion. Judging from the rock assemblage (low-Ti tholeiites, volcanics of the boninite series, Fe–Ti basalts, and tholeiitic andesites), this complex is close to the volcanic associations of suprasubductional complexes or inicial Phanerozoic oceanic island arcs (Shchipansky *et al.*, 1999, 2002).

The second stage was marked by the development of temporarily related calc–alkaline intermediate and acid volcanics in the southern part of the structure, intrusive rocks of the adakite series, including subvolcanic dacites, rhyodacites, rhyolites, and trondhjemites framing the structure in the north and, perhaps, also granodiorites in its southern surroundings. Compositionally and geochemically analogous associations of magmatic rocks are known in some mature Phanerozoic island arcs, where the subducted hot or thickened oceanic plate was both degassed and partially melted (Drummond *et al.*, 1996; Sajona *et al.*, 2000; Prouteau *et al.*, 2000; Samaniego *et al.*, 2002). A distinctive feature of this complex is a laterally heterogeneous distribution of petrogenetically distinct rock types, which determines the asymmetry of the Hisovaara structure: its northern portion consists of subvolcanic and plutonic rocks of exclusively the adakite series, while the southern part is strongly dominated by calc–alkaline volcanic and plutonic rocks with subordinate amounts of subvolcanic adakites. This asymmetry can reflect the lateral heterogeneity of the island arc (Fig. 14), which developed in a specific environment due to higher temperature thermal regimes in the Archean mantle:

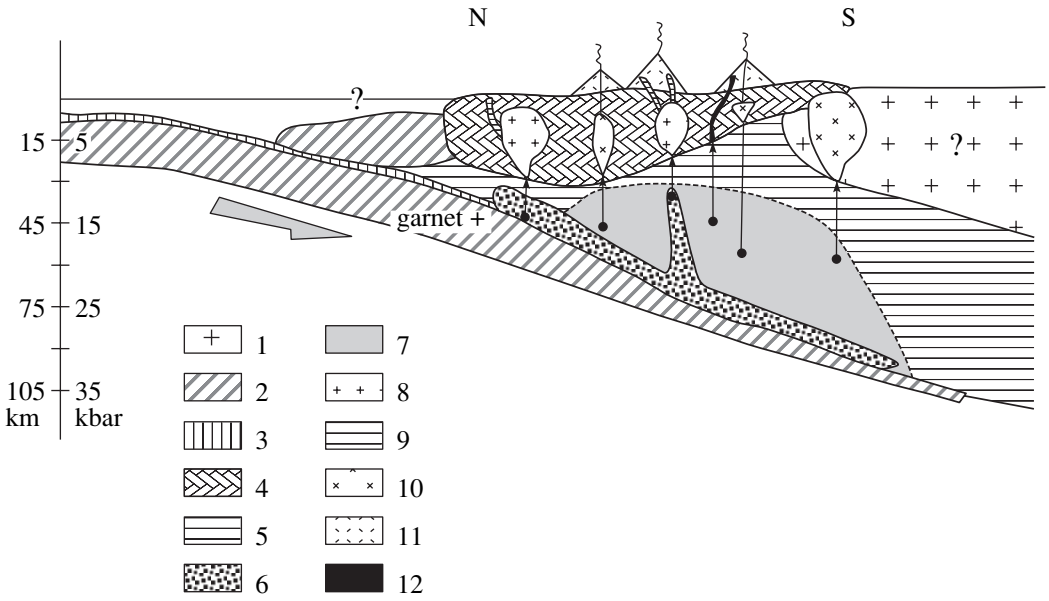

Fig. 14. Hypothetical geodynamic model for the genesis of rocks in the Hisovaara structure.
(1) Continent or a precursor arc complex; (2) oceanic crust; (3) pelagic sediments; (4) initial island arc; (5) unrecycled mantle; (6) adakitic melt derived from the subducted oceanic plate; (7) mantle wedge recycled by fluids and adakitic melts; (8) plutonic adakites; (9) subvolcanic adakites; (10) diorites and granodiorites of the calc–alkaline series; (11) andesites and dacites of the calc–alkaline series; (12) Nb–Ti andesites. The profile is oriented relative to the present-day compass points.

(a) a significant thickness (up to 15–20 km) of the continental crust and a gentle (less than 45°) subduction angle (Sleep and Windley, 1982); and (b) partial melting of the subducted oceanic crust at depths from approximately 40 km (12 kbar) to 100 km (32 kbar) (Rapp *et al.*, 1991). Under these conditions, the partial melting of the downgoing oceanic plate produced, starting from depths of approximately 40 km, adakite melts. In the northern (in modern coordinates), "frontal" portion of the arc, they ascended to the surface without interacting with mantle-wedge rocks and formed the adakitic trondhjemites along the northern periphery of the structure and the subvolcanic rhyodacites. The insignificant contribution of ancient sialic material, as is pointed at by zircon in these rocks, was caused by the involvement of accretionary-prism metasediments in the subduction zone. In deeper parts of the subduction zone, the adakite melts and fluids separating from the slab were largely consumed by the overlying mantle-wedge rocks, a process that triggered the partial melting of the wedge and gave rise to calc–alkaline volcanics of andesite–dacite composition and diorite–granodiorite intrusions in the southern "rear" part of the arc. The volumetrically subordinate and geologically later adakite magmatism in this part of the arc could be related to the local saturation of the mantle wedge with adakite magmas (Samaniego *et al.*, 2002) and/or the development of deep faults as pathways for the ascent of pure adakitic melts.

The island arc seems to have started to develop on a compositionally heterogeneous basement. The predominant rocks of this basement could be complexes of an initial island arc, which are now represented by tholeiitic volcanics in both the northern and the southern part of the structure. Along with this, the rear part of the arc seems to have been located within the influence zone of the earlier sialic crust, as follows from significant amounts of the inherited zircon component in the magmatic zircon of the diorite–granodiorite massif in the southern surrounding of the structure. This structure of the crust in the basement of the island arc could be formed late in the previous evolutionary stage of the Hisovaara structure by the tectonic juxtaposition (accretion or subduction) of the suprasubductional arc complex with an older crustal segment. The latter could be a continental crustal block or, as is discussed below, an older island arc.

Comparison between Isotopic–Geochronological Data on the Hisovaara and Keret' Structures in the Northern Karelian Belt

As was mentioned above, individual structures of the northern Karelian belt show similar tectonic features and compositions of their volcano-sedimentary rocks. The most similar structures of the belt, which are also studied most exhaustively, are the Hisovaara and Keret' structures. The supracrustal sequences of the Keret' structure, as those of the Hisovaara structure considered above, include a lower unit of metavolcanics of mafic and ultramafic composition and an upper unit of intermediate and acid volcanic rocks (which are analogues of, respectively, the northern and southern units of the Hisovaara structure) (Bibikova *et al.*, 1999a). However, the intermediate and acid rocks of the

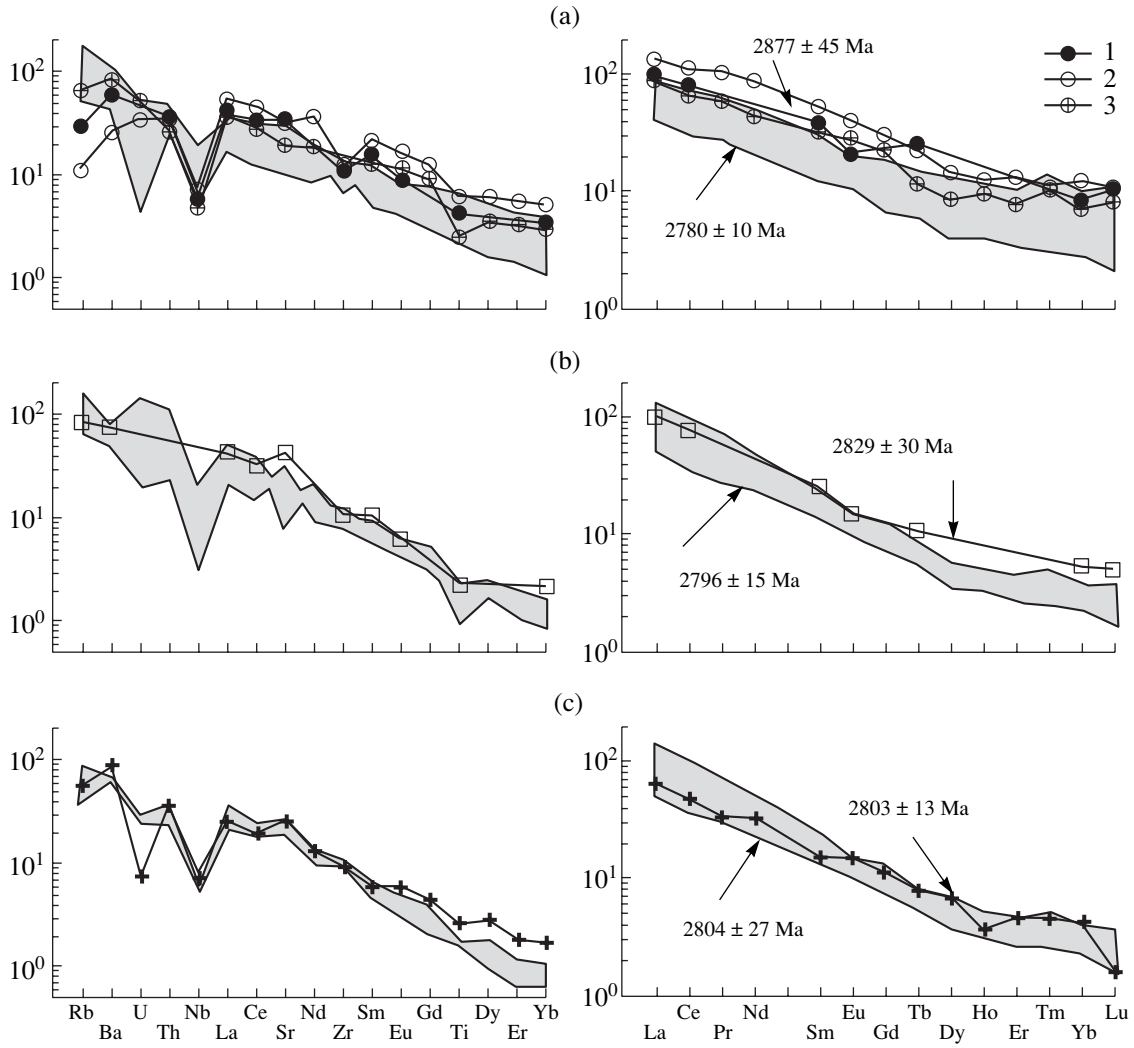

Fig. 15. Comparison of the geochemical characteristics and ages of intermediate and acid rocks the Hisovaara (fields) and Keret' (lines) structures in the northern Karelian belt.

Data on the Keret' structure are borrowed from (Bibikova *et al.*, 1999a). (a) Calc–alkaline volcanics: (1) sample 329-6, (2) sample 329-7, (3) sample 329-15; (b) subvolcanic adakites (sample 455-1); (c) trondhjemites at the northern surrounding of the structure (sample E-12).

two structures, whose geologic settings and petrochemistry are quite similar, were determined to have different isotopic ages (Fig. 15). For example, the high-Al calc–alkaline andesites of the Keret' structure have obviously older zircon isotopic ages (2877 ± 45 Ma) than their petrochemical analogues in the southern portion of the Hisovaara structure (2780 ± 10 Ma). The age obtained for subvolcanic dacite with adakitic signatures from the Keret' structure (2829 ± 30 Ma) is somewhat older than the age of its subvolcanic analogue in the southern part of the Hisovaara structure (2796 ± 15 Ma). At the same time, the syntectonic tonalite pluton of the Keret' structure and similar trondhjemites at the northern periphery of the Hisovaara structure show indistinguishably close isotopic ages: 2803 ± 13 and 2803 ± 27 Ma, respectively. These data testify that calc–alkaline and, perhaps, adakitic volcanism in the Keret' structure occurred somewhat earlier (2.83–2.87 Ga) than analogous magmatism in the Hisovaara structure north of it (2.78–2.80 Ga). At the same time, subvolcanic dacite with adakitic characteristics from the Iringora structure farther to the north in the northern Karelian belt has an age (2782 ± 9 Ma, E.V. Bibikova's unpublished data) indistinguishable from those of its geochemical analogues in the Hisovaara structure. All of these data provide serious evidence for the age heterogeneity of the northern Karelian belt, in which two compositionally similar but different in age complexes can be combined. They could be formed in relation to the evolution of island arcs of different ages.

CONCLUSION

Our data suggest that the volcano-sedimentary and plutonic rock complexes of the Hisovaara structure

were produced over a brief time interval and could be the evolutionary products of the same island arc. The island arc stage is represented by the tholeiitic basalts, volcanics of the boninite series, Fe–Ti basalts (Shchipansky *et al.*, 1999, 2002), and tholeiitic basalts in the northern part of the structure. The U–Pb zircon age of andesites of this stage marks the metamorphic age: 2.78 Ga. The mature-arc complexes, which are dated by the interval of 2.82–2.78 Ga, consist of an association of calc–alkaline and Nb–Ti andesites and adakites, which is typical of the Phanerozoic. The genesis of this association is supposedly related to different grades of interaction between adakitic melts, which were generated by the melting of the hot subducted oceanic plate, and the overlying mantle wedge. Analysis of the geochronologic data points at different ages of the geochemically similar calc–alkaline complexes in two structures of the northern Karelian belt: Hisovaara (2.78–2.80 Ga) and Keret' (2.82–2.88 Ga; Bibikova *et al.*, 1999). This makes it possible to consider the northern Karelian belt to be an accretionary structure with rock associations of at least two island arcs of different ages.

ACKNOWLEDGMENTS

The authors thank V.N Kozhevnikov (Karelian Research Center, Russian Academy of Sciences) for help in the fieldwork and the fruitful discussion of our materials during different stages of this research. The protoliths of the rocks and the character of their geologic relations were discussed in field with M. Marker and P. Ihlen (Geological Survey of Norway). The isotopic geochronologic dating of zircon on a CAMECA 1270 ion microprobe, Nordsim, was made possible by of M. Whitehouse (Swedish Museum of Natural History). The development of the petrological and tectonic models was stimulated by the discussion of our data with H. Martin (Blaise Pascal University, France). The critical comments expressed by G.V. Ledneva (Institute of the Lithosphere, Russian Academy of Sciences) and O.M. Rozen (Geological Institute, Russian Academy of Sciences) helped us to significantly improve the final version of the manuscript.

This study was supported by the Russian Foundation for Basic Research (project nos. 00-05-64701, 99-05-64055, 99-05-65607, 01-05-64674, and 02-05-64989).

REFERENCES

Baker, P.E., Evolution and Classification of Orogenic Volcanic Rocks, in *Andesites*, Thorpe, R.S., Ed., New York: Wiley, 1982, pp. 11–23.

Bibikova, E.V. and Krylov, I.N., The Isotopic Age of Karelian Acid Volcanism, *Dokl. Akad. Nauk SSSR*, 1983, vol. 286, no. 5, pp. 1231–1234.

Bibikova, E.V. and Slabunov, A.I., U–Pb Geochronology and Petrochemistry of the Northern Karelian Diorite–Plagiogranite Batholith, *Geokhimiya*, 1997, no. 11, pp. 1154–1160.

Bibikova, E.V., Ihlen, P.M., and Marker, M., Age of Hydrothermal Alteration Leading to Garnetite and Kyanite Pseudo-Quartzite Formation in the Khizovaara Segment of the Archean Keret Greenstone Belt, Russian Karelia, *6th Workshop of SVEKALAPKO, Europrobe Project*, Abstracts, Oulu, Finland, 2001, p. 15.

Bibikova, E.V., Slabunov, A.I., Bogdanova, S.V., *et al.*, Early Magmatism of the Belomorian Mobile Belt, Baltic Shield: Lateral Zoning and Isotope Age, *Petrologiya*, 1999, vol. 7, no. 2, pp. 115–140.

Bibikova, E.V., Slabunov, A.I., Bogdanova, S.V., and Skiold, T., Tectono–Thermal Evolution of the Earth's Crust in the Karelian and Belomorian Provinces of the Baltic Shield in the Early Precambrian: Evidence from the U–Pb Isotopic Study of Titanite and Rutile, *Geokhimiya*, 1999, no. 8, pp. 842–857.

Borisov, P.A. and Volotovskaya, N.A., The Hisovaara Kyanite Deposit, Karelia, *Sov. Geol.*, 1941, no. 6, pp. 82–86.

Chekulaev, V.P., Levchenkov, O.A., Lobach-Zhuchenko, S.B., and Sergeev, S.A., New Data on the Age Boundaries of the Karelian Archean Complex, in *Obshchie voprosy i printsipy raschleneniya dokembriya* (Precambrian Chronology: General Problems and Principles), Glebovitskii, V.A. and Shemyakin, V.M., Eds., St.-Petersburg: Nauka, 1994, pp. 69–86.

Chekulaev, V.P., Lobach-Zhuchenko, S.B., and Levskii, L.K., Archean Granites in Karelia as Composition and Age Indicators of the Continental Crust, *Geokhimiya*, 1997, no. 8, pp. 805–816.

Drummond, M.S. and Delant, M.J., A Model for Trondhjemite–Tonalite–Dacite Genesis and Crustal Growth via Slab Melting: Archean to Modern Comparisons, *J. Geophys. Res.*, 1990, vol. 95, pp. 21503–21521.

Drummond, M.S., Defant, M.J., and Kepezhinskas, P.K., Petrogenesis of Slab-Derived Trondhjemite–Tonalite–Dacite/Adakite Magmas, *Trans. R. Soc. Edinburgh; Earth Sci.*, 1996, vol. 87, pp. 205–215.

Evensen, N.M., Hamilton, P.J., and O'Nions, R.K., Rare Earth Element Abundances in Chondritic Meteorites, *Geochim. Cosmochim. Acta*, 1978, vol. 42, pp. 1199–1212.

Gaal, G. and Gorbatchev, R., An Outline of the Precambrian Evolution of the Baltic Shield, *Precambrian Res.*, 1987, vol. 35, pp. 15–52.

Glebovitskii, V.A. and Bushmin, S.A., *Usloviya proyavleniya kislotnogo vyshchelachivaniya i metasomatoza pozdneshchelochnoi stadii v metamorficheskikh kompleksakh raznoi glubinnosti* (Conditions of Acid Leaching and Metasomatism during the Late-Alkaline Stage in Metamorphic Complexes at Various Depths), Marakushev, A.A. and Rakcheev, A.D., Eds., Moscow: Nauka, 1982, pp. 118–128.

Hofmann, A.W., Chemical Differentiation of the Earth: The Relationship between Mantle, Continental Crust, and Oceanic Crust, *Earth Planet. Sci. Lett.*, 1988, vol. 90, pp. 297–314.

Huhma, H., Holtta, P., and Paalova, J., Isotopic Studies on the Archean Varpaisjarvi Granulites in Finland, *9th Meeting Association of Eur. Geol. Soc. Precambrian of Europe: Stratigraphy, Structure, Evolution, and Mineralization*, Abstracts, St. Petersburg: Ross. Akad. Nauk, 1995, pp. 42–43.

Ihlen, P.M. and Marker, M., Kyanite-Rich Metasomatic Rocks along Crustal-Scale Shear Zones in the Baltic Shield: Evidence of Shear-Induced Fluid Migration during Tectonic

Dissection of Paleoproterozoic Supracrustal Sequences?, *Svecalapko Europrobe Project*, Abstracts, Repino, Russia, 1998, pp. 25–26.

Je'gouzo, P. and Blais, S., Structural Evidence for Collision Tectonics in the Archean of Eastern Finland, *Geodynamica Acta (Paris)*, 1995, vol. 8, no. 1, pp. 1–12.

Khizovaarskoe kianitovoe pole (Severnaya Kareliya), (The Hisovaara Kyanite Field, Northern Karelia), Petrozavodsk: Karel'skii Filial Akad. Nauk SSSR, 1988.

Kovalenko, A.V. and Rizvanova, N.G., New Geochronological and Isotopic Data on Granitic Magmatism in Central Karelia, in *Geologiya i mineral'nye resursy severo-zapadnoi i tsentral'noi chastei Rossii* (Geology and Mineral Resources of Northwestern and Central Russia), Apatity: 1999, pp. 61–66.

Kozhevnikov, V.N., *Arkheiskie zelenokamennye poyasa Karel'skogo kratona kak akkretsionnye orogeny* (Archean Greenstone Belts in the Karelian Craton as Accretionary Orogenic Belts), Petrozavodsk: Karel'skii Nauch. Tsentr Ross. Akad. Nauk, 2000.

Kozhevnikov, V.N., *Geologiya i geokhimiya severo-karel'skikh zelenokamennykh struktur* (Geology and Geochemistry of Northern Karelian Greenstone Structures), Petrozavodsk: Karel'skii Nauch. Tsentr Ross. Akad. Nauk, 1992.

Kratts, K.O., *Geologiya karelid Karelii* (Geology of the Karelides in Karelia), Moscow: Akad. Nauk SSSR, 1963.

Krogh, T., A Low Contamination Method for Hydrothermal Decomposition of Zircon and Extraction of U and Pb for Isotopic Age Determination, *Geochim. Cosmochim. Acta*, 1973, vol. 37, pp. 485–494.

Krogh, T.E., Improved Accuracy of U–Pb Zircon Ages by the Creation of More Concordant Systems Using an Air Abrasion Technique, *Geochim. Cosmochim. Acta*, 1982, vol. 46, pp. 637–649.

Leat, P.T., Livermore, R.A., Millar, I.L., and Pearce, J.A., Magma Supply in Back-Arc Spreading Center Segment E2, East Scotia Ridge, *J. Petrol.*, 2000, vol. 41, pp. 845–866.

Levchenkov, O.A., Lobach-Zhuchenko, S.B., and Sergeev, S.A., *Geokhronologiya Karel'skoi granit-zelenokamennoi oblasti* (Geochronology of the Karelian Granite–Greenstone Terrane), Levskii, L.K. and Levchenkov, O.A., Eds., Leningrad: Nauka, 1989, pp. 63–72.

Lin, P.-N., Stern, R.J., and Bloomer, S.H., Shoshonitic Volcanism in the Northern Mariana Arc: 2. Large Ion–Lithophile and Rare Earth Element Abundances: Evidence for the Source of Incompatible Element Enrichments in Intraoceanic Arcs, *J. Geophys. Res.*, 1989, vol. 94, pp. 4497–4514.

Lobach-Zhuchenko, S.B., Arestova, N.A., Chekulaev, V.P., *et al.*, Geochemistry and Petrology of 2.40–2.45 Ga Rocks in the Northwestern Belomorian Belt, Fennoscandian Shield, Russia, *Precambrian Res.*, 1998, vol. 92, pp. 223–250.

Lobach-Zhuchenko, S.B., Arestova, N.A., Chekulaev, V.P., *et al.*, The Evolution of the Southothern Vygozero Greenstone Belt in Karelia, *Petrologiya*, 1999, vol. 7, no. 2, pp. 156–173.

Lobach-Zhuchenko, S.B., Arestova, N.A., Mil'kevich, R.I., *et al.*, The Stratigraphic Section of the Kostomuksha Structure in Karelia (Upper Archean) Reconstructed on the Basis of Geochronological, Geochemical, and Isotopic Data, *Stratigr. Geol. Korrelyatsiya*, 2000, vol. 8, no. 4, pp. 3–10.

Lobach-Zhuchenko, S.B., Chekulaev, V.P., Sergeev, S.A., *et al.*, Archaean Rocks from Southeastern Karelia (Karelian Granite–Greenstone Terrain), *Precambrian Res.*, 1993, vol. 62, pp. 375–397.

Lobikov, A.F. and Lobach-Zhuchenko, S.B., Isotope Age of Granites from Palalamba Greenstone Belt, Karelia, *Dokl. Akad. Nauk SSSR*, 1985, vol. 250, no. 3, pp. 729–733.

Lobikov, A.F., On the Age of Early-Karelian Metavolcanic Rocks, Evidence from Lead Isochronous Data, *Tezisy Soveshch. "Problemy izotopnogo datirovaniya"* (Conf. on Isotope Dating, Abstracts), Kiev: Naukova Dumka, 1982, pp. 90–91.

Ludwig, K.B., ISOPLOT Program, *US Geol. Surv. Open File Rep.*, 1991, no. 91.

Luukkonen, E.J., Structural and U–Pb Isotopic Study of Late Archean Migmatitic Gneisses of the Presvecokarelides, Lylyvaara, Eastern Finland, *Trans. R. Soc. Edinburgh; Earth Sci.*, 1985, vol. 76, pp. 401–410.

Martin, H., Adakitic Magmas: Modern Analogues of Archean Granitoids, *Lithos*, 1999, vol. 46, pp. 411–429.

Mattison, J.M., A Study of Complex Discordance in Zircon Using Stepwise Dissolution Technique, *Contrib. Mineral. Petrol.*, 1994, vol. 116, pp. 117–129.

Meijer, A., Anthony, E., and Reagan, M., Petrology of Volcanic Rocks from the Fore-Arc Sites, *Initial Rep. DSDP*, 1982, vol. 60, pp. 709–729.

Mints, M.V., Archean Tectonics of Miniplates, *Geotektonika*, 1998, no. 6, pp. 2–22.

Miyashiro, A., Classification, Characteristics, and Origin of Ophiolites, *J. Geol.*, 1975, vol. 83, pp. 249–281.

Miyashiro, A., Volcanic Rock Series in Island Arcs and Active Continental Margins, *Am. J. Sci.*, 1974, vol. 274, pp. 321–355.

Ovchinnikova, G.V., Matrenichev, V.A., Levchenkov, O.A., *et al.*, U–Pb and Pb–Pb Isotopic Studies of Acid Volcanic Rocks from the Hautavaara Greenstone Structure, Central Karelia, *Petrologiya*, 1994, vol. 2, no. 3, pp. 266–281.

Paavola, J., A Communication on the U–Pb and K–Ar Age Relations of the Archean Basement in the Lapinlahti–Varpaisjarvi Area, Central Finland, *Bull. Geol. Surv. Finland*, 1986, vol. 339, pp. 7–15.

Papunen, H., Halkoaho, T., Tulenheimo, T., and Liimatainen, J., Excursion to the Kuhmo Greenstone Belt, *Geol. Surv. Finland Spec. Pap.*, 1998, vol. 26, pp. 91–106.

Peate, D.W. and Siems, D.F., Causes of Spatial Compositional Variations in Mariana Arc Lavas: Trace Element Evidence, *The Island Arc*, 1998, vol. 7, pp. 479–495.

Prouteau, G., Maury, R.C., Sajona, F.G., *et al.*, Behavior of Niobium, Tantalum, and Other High Field Strength Elements in Adakites and Related Lavas from the Philippines, *The Island Arc*, 2000, vol. 9, pp. 487–498.

Prouteau, G., Scaillet, B., Pichavant, M., and Maury, R.C., Fluid-Present Melting of Ocean Crust in Subduction Zones, *Geology*, 1999, vol. 27, pp. 1111–1114.

Puchtel, I.S., Hofmann, A.W., Amelin, Yu.V., *et al.*, Combined Mantle Plume—Island Arc Model for the Formation of the 2.9 Ga Sumozero–Kenozero Greenstone Belt, SE Baltic Shield: Isotope and Trace Element Constraints, *Geochim. Cosmochim. Acta*, 1999, vol. 63, no. 21, pp. 3579–3595.

Puchtel, I.S., Hofmann, A.W., Mezger, K., *et al.*, Oceanic Plateau Model for Continental Crustal Growth in the Archean: A Case Study from the Kostomuksha Greenstone

Belt, NW Baltic Shield, *Earth Planet. Sci. Lett.*, 1998, vol. 155, pp. 57–74.

Rapp, R.B. and Watson, E.B., Dehydration Melting of Metabasalt at 8–32 Kbar: Implications for Continental Growth and Crust–Mantle Recycling, *J. Petrol.*, 1995, vol. 36, pp. 891–931.

Rapp, R.B., Watson, E.B., and Miller, C.F., Partial Melting of Amphibolite/Eclogite and the Origin of Archean Trondhjemites and Tonalities, *Precambrian Res.*, 1991, vol. 51, pp. 1–25.

Rollingson, H., *Using Geochemical Data: Evaluation, Presentation, Interpretation*, Harlow: Longman, 1993.

Rybakov, S.I. and Kulikov, B.C., *Priroda i dinamika razvitiya arkheiskikh zelenokamennykh poyasov Baltiiskogo shchita* (The Nature and Evolutionary Dynamics of Archean Greenstone Belts in the Baltic Shield), Kuznetsov, V.A., Ed., Novosibirsk: Nauka, 1985, pp. 164–170.

Rybakov, S.I. and Mel'yantsev, N.V., The Hizovaara Paleovolcanic Structure, in *Geologiya dokembriya Severnoi Karelii* (Geology of the Northern Karelian Precambrian), Petrozavodsk, 1986, pp. 16–18.

Rybakov, S.I., *Metamorfizm osadochno-vulkanogennykh formatsii rannego dokembriya* (Metamorphism of Sedimentary–Volcanogenic Associations of the Early Precambrian), Petrozavodsk: Karel. Filial Akad. Nauk SSSR, 1980.

Sajona, F.G., Bellon, H., Maury, R.C., *et al.*, Magmatic Response to Abrupt Changes in Geodynamic Settings: Pliocene–Quaternary Calc–Alkaline and Nb-Enriched Lavas from Mindanao (Philippines), *Tectonophysics*, 1994, vol. 237, pp. 47–72.

Sajona, F.G., Maury, R.C., Prouteau, G., *et al.*, Slab Melt as a Metasomatic Agent in Island Arc Magma Mantle Sources, Negros and Batan (Philippines), *The Island Arc*, 2000, vol. 9, pp. 472–486.

Samaniego, P., Martin, H., Robin, C., and Monzier, M., Transition from Calc–Alkalic to Adakitic Magmatism at Cayambe Volcano, Ecuador: Insights into Slab Melts and Mantle Wedge Interactions, *Geology*, 2000, vol. 30, pp. 967–970.

Samsonov, A.V., Berzin, R.G., Zamozhnyaya, N.G., *et al.*, Growth of the Early Precambrian Crust in Northwestern Karelia, Baltic Shield: The Results of Geological, Petrological, and Deep Seismic (4V Profile) Studies, in *Glubinnoe stroenie zemnoi kory po profilyu 4V (Kem'–Kalevala)* [Deep Structure of the Earth's Crust in 4V Profile (Kem'–Kalevala)], Berzin, R.G. *et al.*, Eds., Karel. Nauch. Tsentr Ross. Akad. Nauk, 2001, pp. 109–143.

Samsonov, A.V., Puchtel, I.S., Shchipansky, A.A., *et al.*, 2.88 Ga Island-Arc Magmatism of the Kamennoozero Greenstone Belt, Eastern Karelia, Russia, *Int. Conf. "Early Precambrian: Genesis and Evolution of the Continental Crust,"* Abstracts, Moscow, 1999a, pp. 150–152.

Samsonov, A.V., Puchtel, I.S., Shchipansky, A.A., *et al.*, Isotope–Geochemical Variations between Felsic Volcanic Rocks from Karelian Greenstone Belts and Some Tectonic Implications, *9th Conf. Eur. Union of Geosci.*, Abstracts, Strasbourg (France), 1997, p. 363.

Samsonov, A.V., Puchtel, I.S., Shchipansky, A.A., and Bibikova, E.V., *2.72 Ga Orthoandesites of the Kostomuksha Greenstone Belt: Petrology and Tectonic Application, Svekalapko Europrobe Project Workshop*, Abstracts, Lammi (Finland), 18–21.11.1999(b), p. 58.

Sergeev, S.A., Geology and Isotopic Geochronology of Granite–Greenstone Archean Complexes in Central and Southeastern Karelia, *Cand. Sci. (Geol.–Min.) Dissertation*, Leningrad: Inst. Geol. Geochronol. Dokembriya, Ross. Akad. Nauk, 1989.

Shcheglov, A.D., Moskaleva, V.N., Markovskii, B.A., *et al.*, *Magmatizm i metallogeniya riftogennykh sistem vostochnoi chasti Baltiiskogo shchita* (Magmatism and Metallogeny of Riftogenic Systems in the Eastern Part of the Baltic Shield), St. Petersburg: Nedra, 1993.

Shchipansky, A.A., Babarina, I.I., Krylov, K.A., *et al.*, The Earth's Most Ancient Ophiolites: The Late-Archean Suprasubductional Complex in the Iringora Structure of the North-Karelian Greenstone Belt, *Dokl. Ross. Akad. Nauk*, 2001, vol. 377, no. 3, pp. 376–380.

Shchipansky, A.A., Samsonov, A.V., Bibikova, E.V., *et al.*, *2.8 Ga Boninite-Hosting Partial Suprasubduction Zone Ophiolite Sequences from the North Karelian Greenstone Belt, NE Baltic Shield, Russia*, Kusky, T., Ed., Amsterdam: Elsevier, 2002 (in press).

Shchipapsky, A.A., Samsonov, A.V., Bogina, M.M., *et al.*, High-Magnesian, Low-Titanium Quartz Amphibolites of the Hisovaara Greenstone Belt, Northern Karelia: Metamorphosed Archean Analogues of Boninites? *Dokl. Ross. Akad. Nauk*, 1999, vol. 365, no. 6, pp. 817–820.

Slabunov, A.I., The Keret' Upper-Archean Granite–Greenstone System of Karelia, *Geotektonika*, 1993, no. 5, pp. 61–74.

Sleep, N.H. and Windley, B.F., Archaean Plate Tectonics: Constraints and Inferences, *J. Geol.*, 1982, vol. 90, pp. 363–380.

Sochevanov, N.N., Arestova, N.A., Matrenichev, V.A., *et al.*, The First Data on Sm–Nd Age of Archean Basalts from the Karelian Granite–Greenstone Terrane, *Dokl. Akad. Nauk SSSR*, 1991, vol. 318, no. 1, pp. 175–180.

Sokolov, D.N., *Gazovaya khromatografiya letuchikh kompleksov metallov* (Gas Chromatography of Volatile Metal Complexes), Moscow: Nauka, 1981.

Sokolov, V.A., *Stratigrafiya dokembriya Karel'skoi ASSR (arkhei, nizhnii proterozoi)* (Precambrian Stratigraphy of Karelian ASSR: Archean and Low Proterozoic), Petrozavodsk: Karel. Filial Akad. Nauk SSSR, 1984.

Stacey, J.S. and Kramers, J.D., Approximation of Terrestrial Lead Isotope Evolution by a Two-Stage Model, *Earth Planet. Sci. Lett.*, 1975, vol. 26, pp. 207–221.

Staudigel, H., Tauxe, L., Gee, J.S., *et al.*, Geochemistry and Intrusive Directions in Sheeted Dikes in the Troodos Ophiolite: Implications for Mid-Ocean Ridge Spreading Centers, *Electronic J. Earth Sci.*, 1999, vol. 1, no. 1999GC000001.

Steiger, R.H. and Jager, E., Subcommission on Geochronology: Convention of the Use of Decay Constants in Geo- and Cosmo-Chronology, *Earth Planet. Sci. Lett.*, 1976, vol. 36, pp. 359–362.

Stern, C.R., Huang, W.-L., and Wyllie, P.J., Basalt–Andesite–Rhyolite–H_2O: Crystallization Intervals with Excess H_2O and H_2O-Undersaturated Liquidus Surfaces to 35 Kbar, with Implications for Magma Genesis, *Earth Planet. Sci. Lett.*, 1975, vol. 28, pp. 189–196.

Svetov, S.A., The Vedlozero–Segozero Greenstone Belt as a Late-Archean Suture: Geological and Geochemical Arguments, *Tezisy Soveshch. "Glubinnoe stroenie i geodinamika Fennoskandii, okrainnykh i vnutriplatformennykh tranzitnykh zon"* (Conf. on Deep Structure and Geodynamics of

Fennoscandia, Marginal and Intraplatorm Transit Zones), Petrozavodsk, 2002, pp. 216–217.

Systra, Yu.I. and Skornyakova, N.I., Deformation of Lopian Formations in the Hizovaara–Keret' Lake, Northern Karelia, *Tezisy dokl. "Strukturnyi analiz kristallicheskikh kompleksov"* (Conf. Structural Analysis of Crystalline Complexes), Moscow, 1986, pp. 70–72.

Systra, Yu.I., *Tektonika Karel'skogo regiona* (Tectonics of the Karelian Region), Petersburg: Nauka, 1991.

Thurston, P.C. and Kozhevnikov, V.N., An Archean Quartz Arenite–Andesite Association in the Eastern Baltic Shield, Russia: Implications for Assemblage Types and Shield History, *Precambrian Res.*, 2000, vol. 101, pp. 313–340.

Vaasjoki, M. and Sakko, M., Isotopic Age Limitations and Genesis of the Greenstone Belts of Finland and Related Ore Deposits, *Symp. on Types and Stages of the Evolution of the Greenstone Belts and Their Metallogeny*, Abstracts, Petrozavodsk: Karel. Nauch. Tsentr Ross. Akad. Nauk, 1991, pp. 17–19.

Vaasjoki, M., Sorjonen-Ward, P., and Lavikainen, S., U–Pb Age Determinations and Sulfide Pb–Pb Characteristics from the Late Archean Hattu Schist Belt, Ilomantsi, Eastern Finland, *Geol. Surv. Finland Spec. Pap.*, 1993, vol. 17, pp. 103–131.

Vidal, Ph., Blais, S., Jahn, B.M., and Capdevila, R., U–Pb and Rb–Sr Systematics of the Suomussalmi Archean Greenstone Belt (Eastern Finland), *Geochim. Cosmochim. Acta*, 1980, vol. 44, no. 12, pp. 2033–2044.

Whitehouse, M., Claesson, S., Sunde, T., and Vestin, J., Ion Microprobe U–Pb Zircon Geochronology and Correlation of Archean Gneisses from the Lewisian Complex of Gruinard Bay, Northwestern Scotland, *Geochim. Cosmochim. Acta*, 1997, vol. 61, pp. 4429–4438.

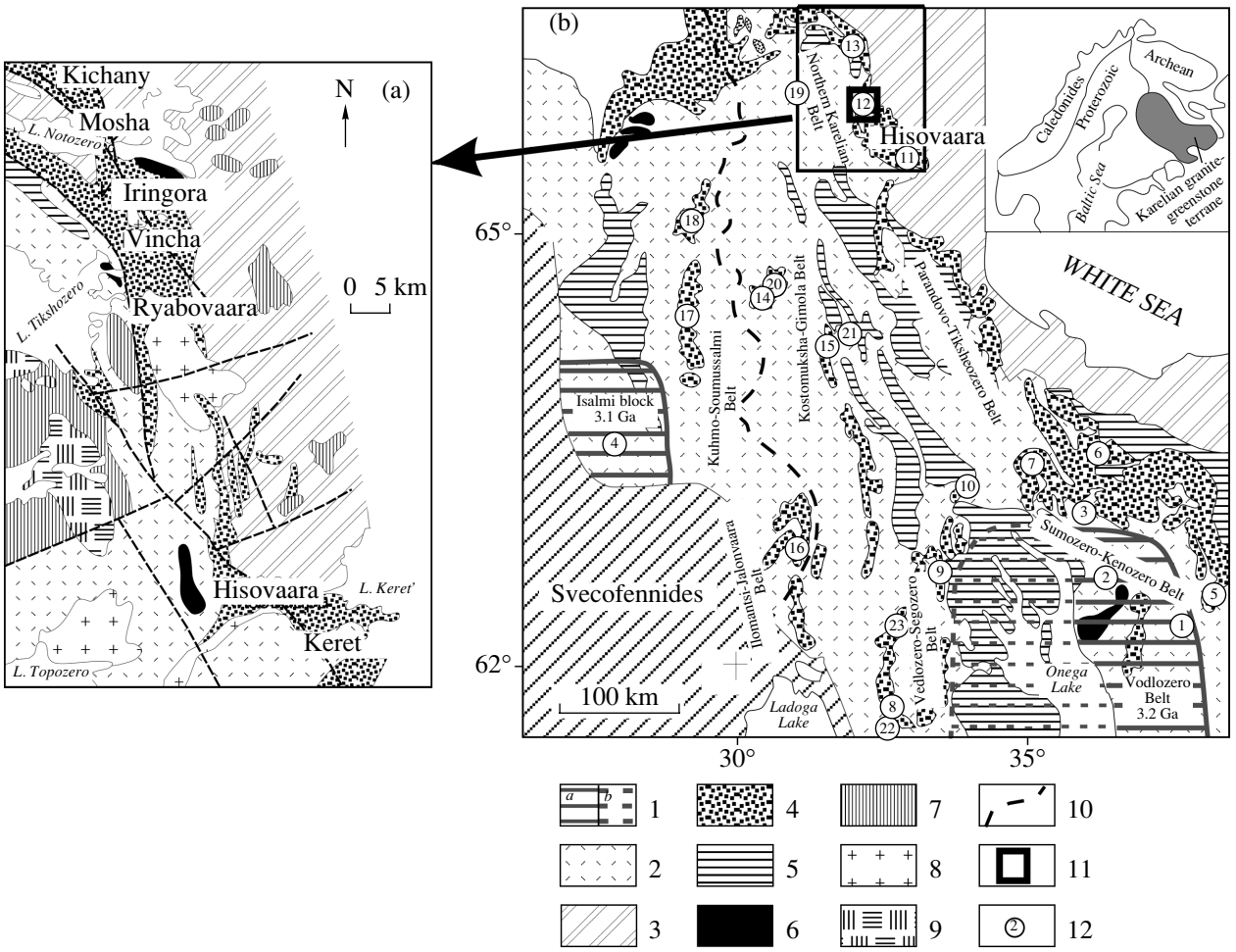

Attempts to reconstruct the tectonic nature of greenstone belt have a long-lasting history. Already during the early stages of their study, these belts were thought to be "protogeosyncline systems" because of their amazing structural and compositional resemblance with Phanerozoic foldbelts (Kratts, 1963). Later, the discovery of komatiites (high-Mg volcanic rocks) led several researchers to conclude that Archean tectonic environments were specific and had no analogues in Phanerozoic time, so that greenstone belts in Karelia have long been ascribed to riftogenic structures, produced during the breakup of the thin sialic crust under the effect of a large mantle plume (Rybakov and Kulikov, 1985). However, materials newly obtained over the past decades forced most researchers to return to actualistic models. Geochronologic evidence testifies to different ages of greenstone belts in the eastern and western Karelian GGT (2.94–2.88 and 2.82–2.80 Ga, respectively), which furnished the basis for the idea that the Archean crust of the Karelian GGT was formed in the process of lateral accretion of these structures from west to east (Mints, 1998). In terms of geochemical and isotopic characteristics, the mafic and ultramafic metavolcanics of the greenstone belts are comparable with post-Archean volcanic associations of various tectonic environments: oceanic crust (Lobach-Zhuchenko, 2002), oceanic plateaus (Puchtel *et al.*, 1998, 1999), initial island arcs (Bibikova *et al.*, 1999a; Shchipansky *et al.*, 1999, 2001, 2002), or back-arc basins (Gaal and Gorbatchev, 1987; Kozhevnikov, 2000). At the same time, the intermediate and acid volcanics of the belts exhibit similarities with the associations of mature island arcs and active continental margins (Gaal and Gorbatchev, 1987; Puchtel *et al.*, 1999; Bibikova *et al.*, 1999a; Kozhevnikov, 2000; Thurston and Kozhevnikov, 2000; Lobach-Zhuchenko, 2000a). All of these data suggest that the greenstone belts combine volcanogenic associations from diverse tectonic environments, which makes them similar to Phanerozoic accretionary belts (Kozhevnikov, 2000).

An important aspect of the problem is the relative ages of and the prototectonic relations between volcanogenic associations within the belts and with the framing TTG-granitoids. In most of the aforementioned papers, these relations are discussed with reference to compositionally contrasting mafic and salic volcanic associations. In several instances, geologic–structural evidence points to an older age of the mafic and ultramafic metavolcanics, although the opposite relations were also obtained (Sokolov, 1984). There are rela-

Fig. 1. Schematic geological map of (a) the Karelian granite–greenstone terrane (modified after Sokolov, 1997) and (b) the northern Karelian belt.

(a) (1) Pre-greenstone sialic blocks: (*a*) observed, (*b*) inferred; (2) granitoid gneisses, migmatites, and plutons; (3) Belomorian Complex of gneisses and amphibolites; (4) Archean greenstone belts; (5) Proterozoic greenstone belts; (6) Proterozoic mafic–ultramafic massifs; (7) Late Archean granitoids; (8) Late Archean garnet–muscovite granites and charnockites; (9) alkaline rocks; (10) state boundaries; (11) study area; (12) sampling sites for U–Pb zircon and Sm–Nd whole-rock isotopic geochronologic dating of Archean rocks.

(b) Circled numerals are **ancient, pre-greenstone blocks**, *Vodlozero block, eastern Karelia.* (1) Area of Lake Vodla: tonalite–trondhjemite gneisses, 3540 ± 60 and 3500 ± 90 Ma, 3140–3115 Ma (Sergeev, 1989; Chekulaev *et al.*, 1997), Sm–Nd T(DM) = 3.2 Ga (Chekulaev *et al.*, 1997); amphibolites 3320 ± 100 and 3307 ± 20 Ma (Sergeev, 1989). (2) Area of Lai Creek–Kal'ya River–Lake Chernoe: tonalitic gneisses, 3156 ± 13 Ma (Chekulaev *et al.*, 1994), 3170 (Chekulaev *et al.*, 1997), Sm–Nd T(DM) = 3.5–3.2 Ga (Lobach-Zhuchenko *et al.*, 1993; Chekulaev *et al.*, 1997); pyroxenite–gabbro–diorite massif, 2976 ± 3 Ma (Chekulaev *et al.*, 1994); diorites, 2971 ± 11 Ma (Lobach-Zhuchenko *et al.*, 1999); tonalites, 2957 ± 23 Ma (Lobach-Zhuchenko *et al.*, 1999); and granodiorites, 2908 ± 12 Ma (Lobach-Zhuchenko *et al.*, 1999). (3) Area of Lake Vyg: tonalite–trondhjemite gneisses, 3210 ± 15 and 3128 ± 11 Ma (Sergeev, 1989); granodioritic gneiss, 3140 Ma, Sm–Nd T(DM) = 3.3 Ga (Chekulaev *et al.*, 1997). (4) *Iisalmi block, eastern Finland*: tonalitic gneisses, 3136 ± 20 and 3095 ± 18 Ma (Paavola, 1986), Sm–Nd T(DM) = 3.2–3.4 Ga (Huhma *et al.*, 1995).

TTG–greenstone belts. *Sumozero–Kenozero belt.* (5) Kenozero structure: basalts, 2916 ± 70 Ma (Sochevanov *et al.*, 1991). (6) Kamennozero structure: basalts and komatiites, 2916 ± 117 Ma (Puchtel *et al.*, 1999); adakitic rhyodacites, 2876 ± 5 Ma (Samsonov *et al.*, 1999); BADR rhyolites, 2875 ± 2 Ma (Puchtel *et al.*, 1999). (7) Shiloss structure: basalts, 2960 ± 15 Ma (Sochevanov *et al.*, 1991); TTG granitoids, 2859 ± 24 Ma (Lobach-Zhuchenko *et al.*, 1999).

Vedlozero–Segozero belt. (8) Hautavaara structure: first-stage dacites 2945 ± 19 Ma (Ovchinnikova *et al.*, 1994), second-stage dacites 2862 ± 45 Ma (Ovchinnikova *et al.*, 1994). (9) Koikary structure: first-stage dacites 2935 ± 20 Ma (Bibikova and Krylov, 1983), second-stage dacites 2859 ± 15 Ma, rhyolites 2876 ± 5 Ma (Samsonov *et al.*, 1997). (10) Oster structure: first-stage basalts and andesites, ~3020 Ma (Lobikov, 1982); second-stage subvolcanic rhyolites, 2830 ± 40 Ma (Lobikov and Lobach-Zhuchenko, 1985), granites, 2876 ± 21 Ma (Kovalenko and Rizvanov, 1999).

Northern Karelian belt. (11) Keret' structure: andesite, 2877 ± 45 Ma (Bibikova *et al.*, 1999); dacite, 2829 ± 30 Ma (Bibikova *et al.*, 1999); TTG tonalite, 2803 ± 13 Ma (Bibikova *et al.*, 1999a). (12) Hisovaara structure: subvolcanic rhyolite (north), 2799 ± 67 Ma (Chekulaev *et al.*, 1994); subvolcanic rhyodacite (south), 2805 ± 42 Ma (Chekulaev *et al.*, 1994). (13) Iringora structure: subvolcanic dacite, 2756 ± 22 Ma (Shchipansky *et al.*, 2001).

Kostomuksha–Gimola belt. (14) Kostomuksha structure: komatiites and basalts, 2843 ± 39 Ma (Puchtel *et al.*, 1997, 1998); rhyolites, 2795 ± 25 Ma; T(DM) = 2.9–3.3 Ga (Samsonov *et al.*, 2001). (15) Bol'sheozero structure: rhyolites, 2730 ± 5 Ma (Samsonov *et al.*, 2001).

Eastern Finnish belt. (16) Ilomantsi structure (Vaasijoki *et al.*, 1993): andesites, 2754 ± 6 Ma; metasedimentary rocks (micaceous schists), 2761 ± 11 Ma; feldspathic graywackes, 2744 ± 19 Ma; acid rock fragments from conglomerate, 2727 ± 14 Ma, 2734 ± 3 Ma; dacite dikes, 2733 ± 10 and 2756 ± 6 Ma; peripheral TTG plutons: tonalites, 2744 ± 6 and 2756 ± 9 Ma; granodiorites, 2724 ± 5 and 2744 ± 3 Ma. (17) Kuhmo structure: acid volcanics, 2.79–2.81 Ga (Papunen *et al.*, 1998); framing granodiorites, 2.24 Ga (Je'gouzo and Blais, 1995); TTG gneisses. 2843 ± 13 Ma (Luukkonen, 1985). (18) Soumussalmi structure: andesites, 2966 ± 9 Ma (Vidal *et al.*, 1980; Vaasijoki and Sakko, 1991).

Late- and post-tectonic granitoids. *Sanukitoid (diorite–tonalite–granodiorite massifs)*: (19) Tavajarvi Massif, 2724 ± 8 Ma (Bibikova and Slabunov, 1997). (20) Taloveis Massif, 2720 ± 15 Ma (Samsonov *et al.*, 1999b). (21) Bol'sheozero Massif, 2706 ± 5 Ma (E.V. Bibikova's unpublished data); (22) Panozero Massif, 2737 ± 10 Ma (Chekulaev *et al.*, 1994). (23) Chalka massif, 2744 ± 5 Ma (Levchenkov *et al.*, 1989). *Granite massifs* (numbers of sites correspond to those for other rocks sampled for dating: (9) Koikary, stratiform postkinematic granite, 2684 ± 30 Ma (Chekulaev *et al.*, 1994), Kostomuksha, Shurlovaara Massif, 2679 ± 8 Ma (Lobach-Zhuchenko *et al.*, 2000).

tively scarce data on the petrogenetic and age heterogeneity of the intermediate and acid volcanics. For instance, the Vedlozero–Segozero belt was determined to contain at least two groups of intermediate and acid metavolcanics with island-arc signatures (Fig. 1) and different ages, a fact implying that the associations of two arcs of different ages were combined within the belt (Svetov, 2002). Finally, it was determined that the two pertogenetically contrasting types of calc–alkaline volcanics [adakite and basalt–andesite–dacite–rhyolite (BADR) series] in the Kamennoozero structure (Sumozero–Kenozero belt) are coeval and were supposedly produced during the same subduction episode under thermal conditions specific for the Archean (Puchtel *et al.*, 1999; Samsonov *et al.*, 1999a). These data give grounds to believe that different greenstone belts in the Karelian GGT are accretionary belts, combining the products of either one or several arc cycles. Obviously, this concept can be validated based on a detailed geochemical and geochronologic study of the intermediate and acid volcanics in different belts of the Karelian GGT. This paper presents the results of such a research on the Hisovaara structure in the northern Karelian belt.

The northern Karelian belt extends as a long discontinuous stripe of supracrustal rocks in the northwestern part of the Karelian GGT, at the boundary with the Belomorian block. The belt includes the following structures (listed proceeding from northwest to southeast): Kichany, Mosha, Iringora, Vincha, Ryabovaara, Hisovaara, and Keret' (Fig. 1), all of which are similar in inner structure and the composition of their mafic–ultramafic and intermediate–acid metavolcanics (Kozhevnikov, 1992). The polymodal character of volcanism in the belt with widespread andesites gives grounds to tectonically interpret this belt as an island